DOI: 10.1002/anie.200601815

Spintronics

Spintronics: A Challenge for Materials Science and Solid-State Chemistry

Claudia Felser, Gerhard H. Fecher, and Benjamin Balke*

Keywords:
half-metallic ferromagnets · magnetic properties · materials science · semiconductors

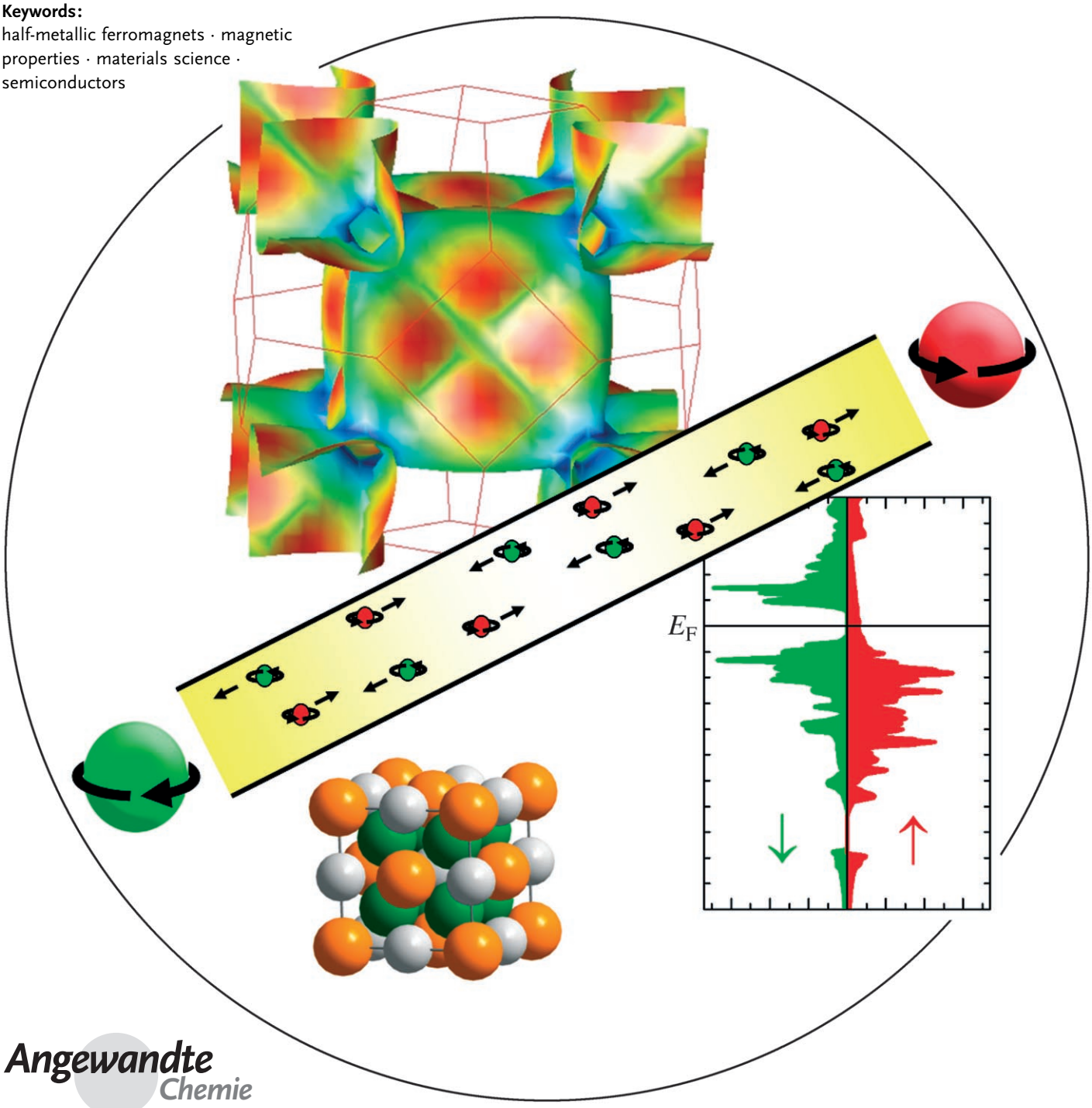

Spintronics is a multidisciplinary field involving physics, chemistry, and engineering, and is a new research area for solid-state scientists. A variety of new materials must be found to satisfy different demands. The search for ferromagnetic semiconductors and stable half-metallic ferromagnets with Curie temperatures higher than room temperature remains a priority for solid-state chemistry. A general understanding of structure–property relationships is a necessary prerequisite for the design of new materials. In this Review, the most important developments in the field of spintronics are described from the point of view of materials science.

From the Contents

1. Introduction

This Review presents the current status of materials research in the field of spin electronics and the related area of magnetoelectronics. Spin electronics, or spintronics, makes use of not only of the charge of electrons, but also their spin. Magnetoelectronics is a subdiscipline dealing with devices that make use of ferromagnetic materials, for example, the read–write heads of computer hard drives. Spintronics also includes semiconductor-based devices. The spin-valve transistor is the most promising example for future applications in quantum computing. The borderline between magnetoelectronics and spintronics is flexible. Magnetic tunneling phenomena, in particular, are a link between the two disciplines.

Section 2 introduces the basic principles of magnetoelectronics and spintronics. The various magnetoresistance effects are explained, and ideas about potential applications are given. Section 3 is devoted to magnetic materials and serves as a basis for the materials-specific Sections. Starting with the classical ferromagnets and the properties of their alloys, the concept of half-metallic ferromagnets is given a broad basis and explained. Basic ideas about materials (covalent half-metals, $C1_b$ and $L2_1$ compounds (*Strukturbericht* designations), ionic half-metals, and ferromagnetic semiconductors) and their bonding characteristics are subsequently introduced.

Specific materials are presented and discussed in Section 4, which is dedicated to materials exhibiting colossal magnetoresistance (see Section 2). Such materials are found among the perovskite manganites, Ruddlesden–Popper compounds, pyrochlores, and Zintl compounds, for example. Copper- and rare-earth-containing compounds are also presented. In Section 5, ferromagnetic semiconductors for spintronics are discussed. In particular, these materials are found in the classes of transition-metal oxides, manganese-doped GaAs and GaN, transparent ferromagnet-doped oxides, B3 and B4 compounds, and doped semiconducting $C1_b$ alloys. Finally, Section 6 concentrates on the materials that exhibit half-metallic ferromagnetism, which are the most promising candidates for applications in spintronics.

2. Magnetoelectronics

Over the last 40 years, the semiconductor industry has been able to continually shrink the size of electronic components on silicon chips, packing ever more performance into computers. The limits of the current technology are reached, when smaller component sizes are prevented by the fundamental physical laws. In the last decade, spintronics has developed as a new approach that has revolutionized the market for electronic devices. Some predicted advantages of this new technology are the nonvolatility of data storage, the increased speed of data processing, the high storage density, and the low energy consumption.

To exploit the full potential of spintronics, the development of new magnetic materials, magnetic semiconductors, and half-metallic ferromagnets is necessary. Half-metallic ferromagnets meet all the requirements of spintronics, as a result of their exceptional electronic structure. These materials behave like metals with respect to the electrons of one spin direction and like semiconductors with respect to the electrons of the other spin direction. CrO_2, perovskite manganites, and many Heusler compounds are half-metallic ferromagnets. Ferromagnetic semiconductors with Curie temperatures higher than room temperature are not yet known.

The primary focus of this Review is on the materials-science aspects, including the basic physical principles, of spintronics and, in particular, magnetoelectronics. In the following Section, a short explanation of the basic spintronic

[*] Prof. Dr. C. Felser, Dr. G. H. Fecher, B. Balke
Institut für Anorganische Chemie und Analytische Chemie
Johannes Gutenberg-Universität Mainz
55099 Mainz (Germany)
Fax: (+49) 6131-3926267
E-mail: felser@uni-mainz.de

and magnetoelectronic effects will be given to introduce this interesting field and to clarify which demands the materials must fulfill.

2.1. Spin Current

All currently available spin-based devices are magnetic memory devices or sensors that use the electron spin to store information. Just as conventional electronic devices require charge currents, spin-based electronic (spintronic) devices require spin currents.[1] Unfortunately, it is very difficult to generate, transport, and detect spin currents. Sharma gave an easily understandable explanation of what is meant by a spin current.[2] Consider an electron current that flows through a wire and contains electrons of only one spin direction, say spin-up-polarized electrons. Add to this current a similar current flowing in the opposite direction in which all electrons are spin-down-polarized. The theoretical result is a current of spins only, without any net particle transfer (Figure 1).

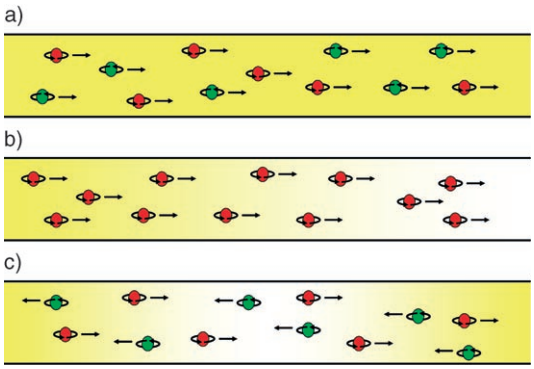

Figure 1. a) A regular charge current, b) a spin and charge current, and c) a pure spin current through a wire. The spin (red or green) and direction of movement of the electrons are indicated.

A spin current (Figure 1c) differs from a charge current (Figure 1a) in some important ways. For a spin current, the ohmic resistivity is suppressed, as no electrons and, thus, no charges are transported. In addition, the spin current is invariant under time reversal: if a clock ran backwards, the spin current would still flow in the same direction. Furthermore, the spin current is associated with a spin flow that is a vector quantity (angular momentum). This circumstance allows quantum information to be transported through semiconducting structures, as in quantum optics using polarized light.

A current that uses not only the electron charge, but also the spin as a transport property requires new types of materials that are completely spin-polarized. In 1983, de Groot et al. defined a fully spin-polarized compound as a half-metallic ferromagnet (HMF).[3] Half-metallic ferromagnets have a band gap at the Fermi energy E_F (the energy that separates the occupied and unoccupied states in extended solids) with respect to the electrons of one spin direction, whereas they are metallic with respect to the electrons of the opposite spin direction (Figure 2). This situation allows a completely polarized current.[3]

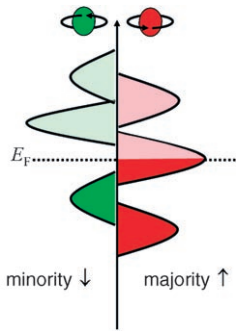

Figure 2. Schematic DOS curve for a half-metallic ferromagnet. In this case, the band gap occurs in the minority DOS (left).

2.2. Magnetoresistance

The basic effect of magnetoelectronics is magnetoresistance (MR), which is generally defined as the ratio of the resistance of a material in the absence a magnetic field to its resistance in a magnetic field. A large change in the electrical resistance in response to an applied magnetic field is of technological relevance for the development of magnetic sensors and memories. The search for new materials and better devices is important because a larger MR effect is necessary for applications.

Claudia Felser earned her diploma in chemistry at the University of Köln in 1989 and completed her doctorate there in 1994. After postdoctoral fellowships at the MPI in Stuttgart and the CNRS in Nantes (France), she joined the University of Mainz. She was a visiting scientist at Princeton University (USA) and a visiting professor at the University of Caen (France), and then became a full professor at the University of Mainz in 2003. She is the chair of the DFG research group "New Materials with High Spin Polarization" and is the coordinator of the Graduate School of Excellence of Rhineland-Palatinate. In 2001, she was honored with the "Landesverdienstorden" for her work in schools.

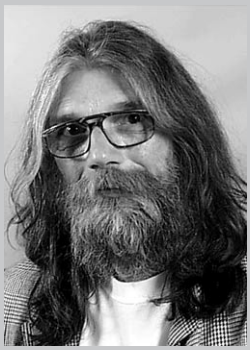

Gerhard H. Fecher earned his diploma in physics at the University of Kassel in 1985 and completed his doctorate at the University of Bielefeld in 1990. After a postdoctoral stay in Bielefeld, he was a research associate at the University of Mainz and at the University of Münster. He also spent a year as a visiting scientist at the Institute of Physics of the Academia Sinica in Taipei (Taiwan). His research focuses on spectroscopic methods at synchrotrons. He is currently a senior scientist in the Materials Science Group of the Institute of Inorganic and Analytical Chemistry at the University of Mainz.

Two definitions of MR ($\Delta R/R$) have been used in the literature. In the first, the MR, which cannot exceed 100%, is defined according to Equation (1), where $R_{\uparrow\downarrow}$ and $R_{\uparrow\uparrow}$ are the

$$\Delta R/R = (R_{\uparrow\downarrow} - R_{\uparrow\uparrow})/R_{\uparrow\downarrow} \quad (1)$$

resistance for antiparallel and parallel alignments of the magnetizations in two adjacent magnetic layers (Figure 3).

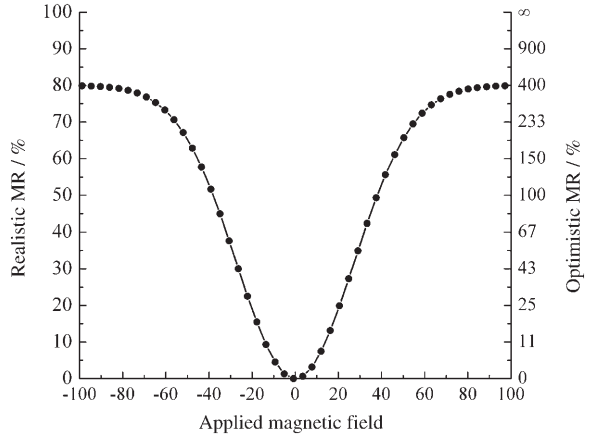

Figure 3. Field (arbitrary units) dependence of the realistic and optimistic MR of a multilayer device consisting of ferromagnetic layers separated by a nonmagnetic layer.

For the comparison of small values, the optimistic definition of MR is advantageous; according to Equation (2), the MR is

$$\Delta R/R = (R_{\uparrow\downarrow} - R_{\uparrow\uparrow})/R_{\uparrow\uparrow} \quad (2)$$

infinite for fully polarized electrodes. In this Review, the realistic definition is used when the MR is lower than 95%. When the MR is higher than 95%, the optimistic definition is used to allow better comparison.

Anisotropic magnetoresistance (AMR), the first MR effect reported, was discovered in 1857 by W. Thomson (Lord Kelvin).[4] This anisotropic effect is small (ca. 3%) and depends on the Fermi surface of the material. From the time of its discovery until 1988, AMR was the most technologically important component of the MR of ferromagnets. The AMR effect has been applied in the fabrication of magnetic sensors and readout heads for magnetic hard disks.

Benjamin Balke earned a degree in chemistry and mathematics at the University of Mainz in 2004. He is currently carrying out doctoral research on the synthesis and photoemission of Heusler compounds as new materials for spintronics under the supervision of Prof. Claudia Felser at the Institute of Inorganic and Analytical Chemistry at the University of Mainz.

2.2.1 *Giant Magnetoresistance*

A breakthrough occurred in 1988 when Grünberg et al.,[5] and Fert et al.[6] independently discovered giant magnetoresistance (GMR), which is ten times larger than AMR. This discovery led to an explosion of research in the field of GMR comparable to that experienced in the field of high-temperature superconductivity. The GMR effect is observed in multilayer systems consisting of alternating magnetic and nonmagnetic layers. It is used in magnetic sensors and in nearly all hard-disk read heads.

Figure 4 shows an example of such an Fe–Cr multilayer system.[6] With the application of a magnetic field, the

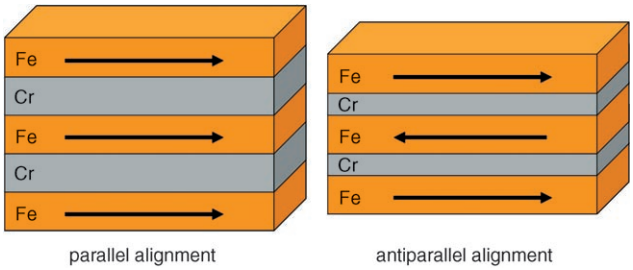

Figure 4. An Fe–Cr multilayer system with ferromagnetic (left) or antiferromagnetic (right) exchange coupling between the iron layers.

resistance of the sample can be suppressed by orders of magnitude. Depending on the thickness of the chromium layers, the interlayer exchange coupling between the iron layers changes from ferromagnetic (parallel) to antiferromagnetic (antiparallel). Measurements of the electrical resistance show that when the exchange coupling is antiferromagnetic, the resistance is high. When a magnetic field is applied, the resistivity drops significantly, as the relative alignment of the magnetization in neighboring iron layers goes from antiparallel to parallel. When an electrical field is applied, the spin-oriented electrons of the iron layers accelerate until they encounter a scattering center. Provided that the interlayer thickness is smaller than the coherence length of the electron, the electron arrives at the interface of the neighboring ferromagnetic layer with its initial spin orientation. In the case of ferromagnetically coupled iron layers, the arriving electron has a high probability of entering the adjacent layer because its spin orientation matches that of the layer. If the exchange coupling is antiferromagnetic, the electron is scattered at the interface, because its opposite spin orientation prevents it from penetrating the layer; a high resistance results. The GMR of an Fe–Cr multilayer with 9-Å-thick chromium layers can reach 79% at 4 K and small fields, and is still 20% at room temperature.[6]

Read heads and magnetic sensors consist of artificial multilayers of alternating thin films of ferromagnetic and nonmagnetic metals. These devices were introduced by IBM in 1997, and the market for them is now estimated to be approximately one billion dollars per year.[7] Figure 5 shows a typical configuration for the measurement of GMR. The current can be either perpendicular (current perpendicular to the plane (CPP)) or parallel (current in the plane (CIP)) to

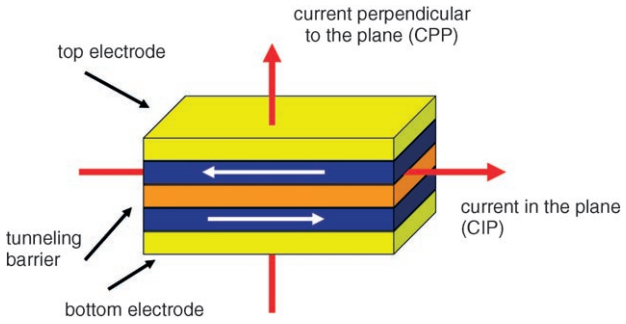

Figure 5. A typical multilayer configuration for the measurement of GMR. The red arrows indicate the direction of the current in the CIP and CPP configurations. The white arrows indicate the exchange coupling between the magnetic layers (blue).

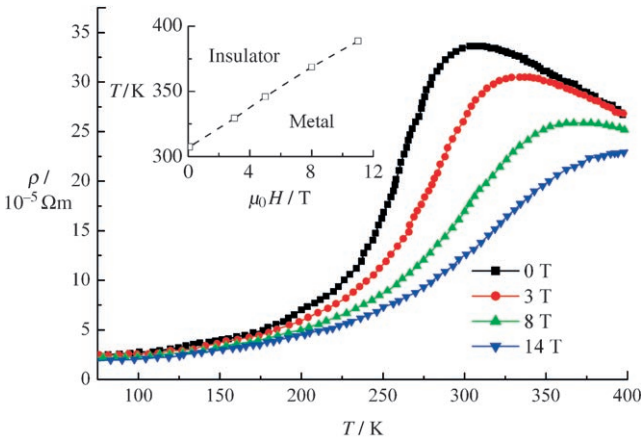

Figure 6. Temperature and field dependence of the resistivity of a thin film of $La_{0.9}Sr_{0.1}MnO_3$ (inset: temperature–field phase diagram; the dashed line is the metal–insulator boundary).[11]

the interfaces. The GMR effect was originally discovered in a CIP configuration; however an even larger effect is found for the CPP configuration.

A spin valve consists of two ferromagnetic layers sandwiching a thin nonmagnetic layer. One of the magnetic layers consists of a hard magnetic material, and its magnetization is insensitive to moderate magnetic fields (pinned); the second magnetic layer consists of a soft magnetic material, and its magnetization can be easily altered by the application of small magnetic fields (free).

2.2.2. *Colossal Magnetoresistance*

In 1993, von Helmolt et al.[8] and, somewhat later, Jin et al.[9] discovered an even larger MR effect in mixed-valence manganese perovskites: colossal magnetoresistance (CMR).

In general, the resistance of a bulk ferromagnetic material is reduced at low temperatures (deviating from the resistance curve of a nonmagnetic metal). Near the Curie temperature (temperature of ferromagnetic ordering), the resistance increases, owing to the scattering of the conduction electrons by spin disorder. Scattering by spin fluctuations is usually a small effect and, in transition metals, resistance changes of only a few percent occur near the Curie temperature. The magnitude of the CMR observed for the perovskite manganites cannot be explained by the scattering of conduction electrons; rather, it is the result of a temperature-dependent metal–insulator transition.

The most famous system is based on $LaMnO_3$ and is described in detail in reference [10]. Most manganites that exhibit CMR belong to the perovskite family. When lanthanum is partially substituted by an alkaline-earth cation, the compound becomes metallic and a large negative MR is observed. Unsubstituted $LaMnO_3$, which contains Mn^{3+}, is antiferromagnetic and does not exhibit CMR. $CaMnO_3$ contains only Mn^{4+} and is also an antiferromagnetic insulator. Upon substitution of lanthanum by calcium to a concentration of $x = 0.2$–0.4, $La_{1-x}Ca_xMnO_3$ becomes mixed-valent and ferromagnetic, and exhibits a sharp drop in resistance as a result of a unique type of metal (low temperatures)–insulator (high temperatures) transition (Figure 6). This family of manganites exhibits an exceptionally rich variety of physical properties in which electronic correlations, and spin and orbital ordering play an essential roles.

A number of systems other than the perovskite manganites also exhibit CMR, including the perovskite-derived Ruddlesden–Popper phases $RE_{1+x}Sr_{2-x}Mn_2O_7$ (RE = trivalent rare earth),[12] perovskite cobalt oxides,[13] pyrochlore thallium or indium manganites,[14] spinels such as $Fe_{0.5}Cu_{0.5}Cr_2S_4$,[15] 14-1-11 phases such as $Eu_{13.97}Gd_{0.03}MnSb_{11}$,[16] $Mn_{1-x}Fe_xS$,[17] and the layered rare-earth iodide GdI_2.[18] CMR has long been known in EuO,[19] in $Gd_{3-x}S_4$,[20] and in a few other rare-earth compounds. Of the elements, gadolinium metal exhibits the largest negative MR,[21] which, however, is much smaller than that of the perovskite manganese oxides and is not associated with a metal–insulator transition. The families of compounds exhibiting CMR will be discussed in detail below.

Although the MR effect is large in the perovskite manganese oxides, neither the sensitivity (MR in low fields) nor the temperature dependence (small MR at room temperature) is sufficient for applications. Nevertheless, CMR systems are still the subject of considerable attention, because $La_{0.7}AE_{0.3}MnO_3$ (AE = Ca, Sr, Ba),[9] GdI_2,[17,18] and $Eu_{13.97}Gd_{0.03}MnSb_{11}$[22,23] are half-metallic ferromagnets. It is, therefore, assumed that a compound that exhibits CMR also exhibits a high spin polarization of the conduction electrons. The spin polarization of a material is defined as the difference between the numbers of majority (spin-up, ↑) and minority (spin-down, ↓) electrons at the Fermi energy. The maximum spin polarization is 100% (see Section 2.2.3).

2.2.3. *Tunnel Magnetoresistance*

The use of half-metallic electrodes in spin valves or in magnetic tunnel junctions (MTJs) results in a pronounced increase in MR. As illustrated in Figure 7, a tunnel junction is a device in which a pinned magnetic layer and a free magnetic layer are separated by a very thin insulating layer, commonly Al_2O_3. The effect is based on the tunneling of electrons through the insulating barrier and is called tunnel magnetoresistance (TMR; described in detail in reference [24]). Early

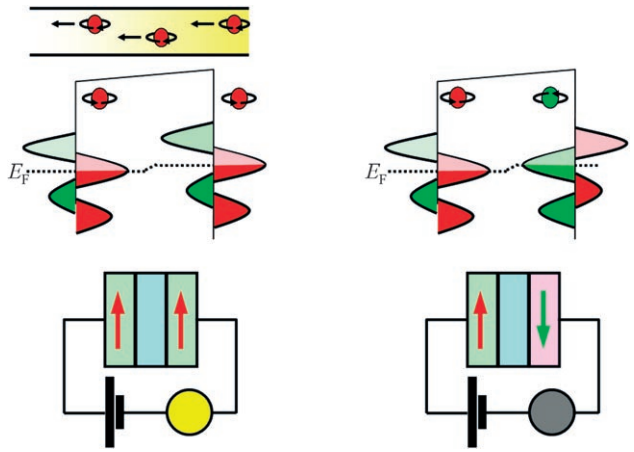

Figure 7. A typical TMR device consisting of a pinned magnetic layer (green) and a free magnetic layer (green or pink) separated by an insulating layer (blue). When the exchange coupling between the pinned and free layers is ferromagnetic, a current flows (left). The DOS curves of the half-metallic magnetic layers are shown above them.

investigations of spin-dependent tunneling were performed by Tedrow and Meservey,[25] Jullière,[26] and Maekawa and Gäfvert in the 1970s.[27] Twenty years later, however, the first large TMR at room temperature was observed by Moodera et al.,[28] and Miyazaki and Tezuka.[29] In the Jullière model,[26] the TMR of a junction is related to the spin polarizations of the two electrodes, P_1 and P_2, according to Equation (3). The

$$\Delta R/R_{TMR} = 2P_1P_2/(1+P_1P_2), \quad (3)$$

spin polarization P is defined by Equation (4), where $N_\uparrow$ and

$$P = (N_\uparrow - N_\downarrow)/(N_\uparrow + N_\downarrow) \quad (4)$$

$N_\downarrow$ are the densities of the majority and the minority electrons at the Fermi energy.

Although the Jullière model is a simple approximation for the tunnel effect, it is commonly used to estimate the spin polarization of electrodes. High spin polarization is required for large TMR. The largest TMR yet reported, 1800%, was measured by Fert et al. for a tunnel junction with a perovskite manganite electrode. This value corresponds to an electrode spin polarization of at least 95%, but unfortunately only at 4 K.[30] Significant progress has recently been achieved with crystalline MgO tunnel barriers: TMR of greater than 400% has been reached at room temperature.[31–33]

2.2.4. *Powder Magnetoresistance*

The powder magnetoresistance (PMR) experiment is a variant of the TMR experiment in which point contacts are made between the grains of a powder of a half-metallic material. The experiment is easy to perform and is a simple way to determine the spin polarization.[34] In the experiment, a powder of a supposedly half-metallic material is compressed into a compact pellet. In the nonmagnetized state, the magnetic orientation of the grains is random, and the resistance is high. When an external magnetic field is applied, the magnetic domains of the grains orient themselves along the direction of the field, leading to a decrease in resistance. Upon cycling the magnetic field, a typical butterfly curve with a maximum at the coercive field is traced for the PMR and the resistance of a powder sample (Figure 8). The contacts

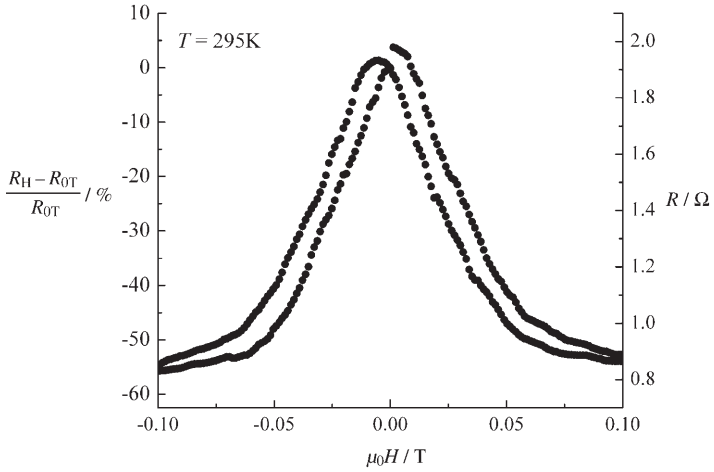

Figure 8. Field dependence of the PMR (R_H and R_0 are the resistance in a magnetic field and in zero field, respectively) and resistance of $Co_2Cr_{0.6}Fe_{0.4}Al + 15\%\ Al_2O_3$ at room temperature (for a complete field cycle).

between the powder grains are typically a mixture of tunnel barriers and ballistic point contacts, and the resistance is determined by the most conductive paths through the maze. It is often helpful to dilute the conducting magnetic powder with an insulating nonmagnetic powder of similar particle size.[34] This extrinsic grain-boundary MR is observed for conducting oxides, such as CrO_2, $Tl_2Mn_2O_7$, Fe_3O_4, ordered double perovskites such as Sr_2FeMoO_6,[35] and $La_{1+x}Sr_{2-x}Mn_2O_7$.[36] In addition, a PMR of 30% was found for powder samples of the Heusler compound $Co_2Cr_{0.6}Fe_{0.4}Al$ in low magnetic fields.[37,38]

2.2.5. *Granular Magnetoresistance*

Granular MR is observed in granular magnetic materials and is related to GMR.[39] A granular-MR material consists of a metallic matrix (copper or silver) with magnetic inclusions. The same effect is also sometimes observed for ordered alloys with magnetic superstructures.[40,41] In these systems, the field dependence of the MR is similar to that for a multilayer GMR system; however, the curves differ at high fields, as saturation is not reached for the granular system. The reason for this behavior is the inhomogeneous particle size distribution of the ferromagnetic inclusions (Figure 9). The magnetization of large particles (with diameters greater than 5 nm) can be easily altered, unlike that of small particles.

2.3. *Spin Injection*

Another possible application of spintronics is based on the spin injection of a spin-polarized current into a semiconductor

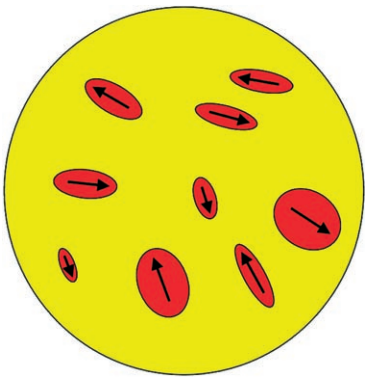

Figure 9. Magnetic inclusions (red, arrows indicate magnetization direction) in a granular sample in the absence of an external magnetic field. If a magnetic field is applied, the magnetization of the particles will align with the field direction, leading to granular MR.

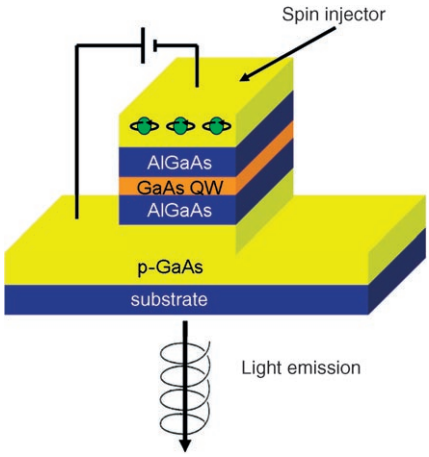

Figure 10. Cross section of a spin-LED based on an AlGaAs–GaAs quantum well (QW) multilayer system. When spin-polarized electrons are injected into the system, the emitted light is circularly polarized.

system.[42] When electrons from a ferromagnet are injected into a nonmagnetic material, they can retain their spin polarization over a certain distance. The prerequisites for this retention of spin polarization are successful spin injection, spin transport within the semiconductor with a spin diffusion length of several microns, spin lifetimes greater than 100 ns, and finally, successful spin detection.[43] The best-suited material would be a ferromagnetic semiconductor with a Curie temperature far above room temperature. Semiconductors doped with small amounts of ferromagnetic impurities, such as manganese, exhibit room-temperature ferromagnetism and are called diluted magnetic semiconductors (DSMs). These materials exhibit both semiconducting and magnetic properties, and have a large potential for application in spintronic devices. Major progress in this field was achieved by Ohno et al.[44,45] and Awshalom et al.,[42] who demonstrated that electrons can retain their spin polarization over unexpectedly long times and distances.[42,46,47] Important devices based on DMSs are spin-polarized light-emitting diodes (spin-LEDs) and spin-polarized field-effect transistors (spin-FETs).[43] A spin-FET is a FET in which the source and the drain are ferromagnetic materials intended for the injection and detection of spin-polarized currents. The conduction depends on the spin orientation and can be controlled by the gate voltage. A spin-LED is illustrated in Figure 10; when spin-polarized electrons are injected into the semiconductor, the emitted light is circularly polarized.

3. Magnetic Materials

Now that the relevant MR effects have been briefly explained, we turn our focus to the materials themselves: half-metallic ferromagnets, compounds that exhibit CMR, and ferromagnetic semiconductors.

3.1. Normal Ferromagnetic Metals

Most ferromagnetic materials are metals. The ferromagnetic transition metals are iron, cobalt, and nickel. All three elements exhibit high Curie temperatures (Fe: $T_C = 1039$ K, Co: $T_C = 1394$ K, Ni: $T_C = 633$ K); however, they are not half-metallic. The rare-earth metals gadolinium ($T_C = 288$ K), dysprosium, and terbium are ferromagnetic, as are a large number of metallic alloys and compounds. In general, half-metallic ferromagnets are rare because of their unique electronic structure.

As can be seen in Figure 11, right, for a normal (paramagnetic) metal, such as copper, there is no difference in the numbers of majority and minority electrons. For the transition elements, the bands of the valence s, p, and d electrons overlap because of different band dispersions. As shown in Figure 11, middle, for a ferromagnetic metal, such as nickel, the electronic structure is spin-polarized, and the numbers of majority and minority electrons differ. The 3d bands of nickel are fully spin-polarized, and the majority 3d band is completely filled by five electrons. The Fermi level crosses the majority 4s band, which is nearly unpolarized, resulting in a finite density of states (DOS) for electrons of both spin directions at the Fermi energy. The difference in the DOS at

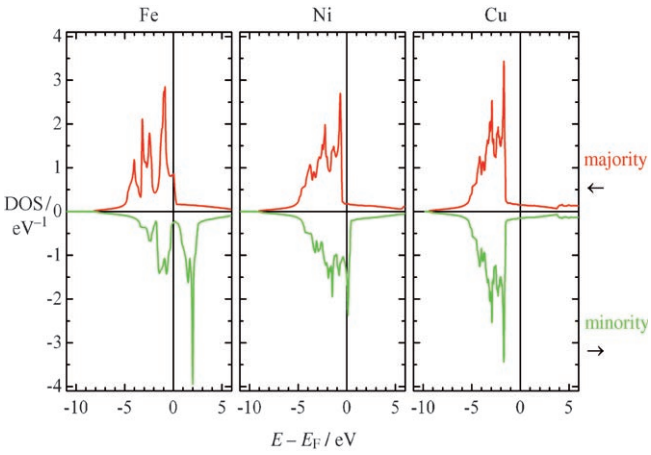

Figure 11. Spin-polarized DOS curves for the ferromagnetic metals iron (bcc) and nickel (fcc) compared to that for the paramagnetic metal copper (fcc).

the Fermi level leads to differing electrical conductance for the majority electrons and the minority electrons, resulting in a spin-polarized current. However, the 4s electrons carry most of the majority current. Such materials, with filled majority d bands, are called strong ferromagnets (examples are cobalt, nickel, and their alloys).[48]

In iron, as shown in Figure 11, left, the situation changes, and the 3d electrons of both spin directions are responsible for conduction. Such materials, with only partially filled majority d bands, are called weak ferromagnets (examples are iron, and Fe–V or Fe–Cr alloys). Note that the terms "strong" and "weak" ferromagnetism are not simply related to the magnitude of the magnetic moment (which is indeed higher in iron than in nickel). For iron, there is a minimum in the minority DOS curve at the Fermi level; however the DOS does not vanish, because of hybridization between the 3d and 4s bands.

To have exclusively either minority or majority electrons at the Fermi level, the 3d and 4s bands of the ferromagnetic transition element must be reordered. As illustrated in Figure 2, the DOS at the Fermi level must have a real gap in one spin direction for the compound to be a half-metallic ferromagnet. The occurrence of a band gap in the overall band structure of an element or a compound is, therefore, a prerequisite for a half-metallic ferromagnet.

There are two ways to produce such a band gap in the electronic structure of a ferromagnetic compound. For an ionic half-metal, the bottom of the 4s band is raised above the Fermi energy, or the Fermi level is lowered below the bottom of the 4s band. Alternatively, a band gap may arise through covalent bonding. For covalent intermetallic compounds, the hybridization of orbitals on different atoms leads to the separation of the bonding and antibonding states by a band gap. In either case, it is necessary to go from a pure element to an alloy or compound. All half-metallic ferromagnets contain more than one element; some are stoichiometric compounds, whereas others (such as the perovskite manganites) are solid solutions.

Note that there is no relation between a half-metal and a semimetal. Semimetals, of which graphite and bismuth are textbook examples, have small and equal numbers of conduction electrons and holes (ca. 0.01 per atom) arising from a small overlap of the valence and conduction bands in their electronic structures. This situation leads to anisotropic conduction. In contrast, the electronic structure of a half-metal has a real band gap in one spin direction (like a semiconductor), but no band gap in the other spin direction (like a metal).

3.2. The Slater–Pauling Rule

Slater[49] and Pauling[50] independently found that the magnetic moments per atom m of the 3d transition elements and their binary alloys could be estimated by the mean number of valence electrons per atom n_V. As described by Kübler,[48] a plot of m versus n_V is called a Slater–Pauling curve. Figure 12 shows the Slater–Pauling curve for first-row transition metals and some of their alloys; the Heusler compound Co_2MnSi and the $C1_b$ compound NiMnSb are included for comparison.

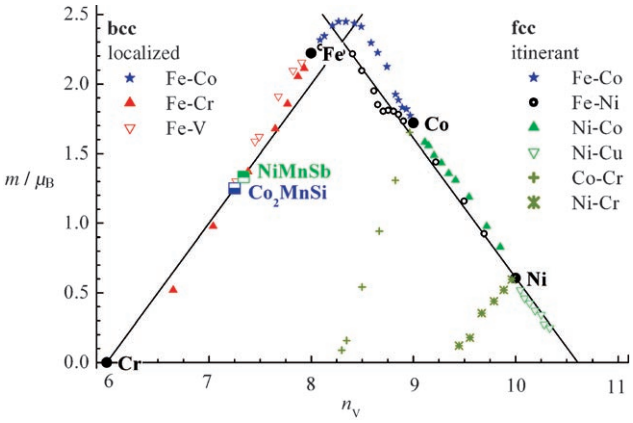

Figure 12. Comparison of the experimental magnetic moments per atom for 3d transition metals and some of their binary alloys to the Slater–Pauling rule (lines). NiMnSb and Co_2MnSi are included for comparison.

On the basis of the Slater–Pauling curve, materials are separated into two regions. The first region of the curve corresponds to high valence-electron concentrations ($n_V \geq 8$) and is the region of itinerant magnetism. For the most part, materials with close-packed structures (face-centered cubic (fcc) or hexagonal close-packed (hcp)) are found in this region. The second region of the curve, in which mainly materials with body-centered cubic (bcc) or bcc-derived structures are found, corresponds to low valence-electron concentrations ($n_V \leq 8$) and is the region of localized magnetism. Iron is located at the border to this region.

From the definition of the magnetic moment ($m = n_\uparrow - n_\downarrow$, in units of the Bohr magneton μ_B), and the concentration of valence electrons ($n_V = n_\uparrow + n_\downarrow$), it is easy to show that the Slater–Pauling rule for the part of the curve describing itinerant magnetism is given by Equation (5). For filled

$$m = 2n_\uparrow - n_V = 2(n_{d\uparrow} + n_{sp\uparrow}) - n_V \quad (5)$$

majority d bands (as for nickel, Figure 11, middle), $n_{d\uparrow} = 5$, giving Equation (6).

$$m = 10 - n_V + 2n_{sp\uparrow} \quad (6)$$

Slater and Pauling found that the number of occupied s–p states is $n_{sp} = 2n_{sp\uparrow} \approx 0.6$, if the electrons are not polarized. This result explains the itinerant part of the curve, as well as the fact that for nickel the magnetic moment is approximately $0.6\mu_B$. Some alloys do not seem to follow the expected curve (Co–Cr and Ni–Cr in Figure 12). Malozemoff et al. demonstrated that the high valence-electron concentration part of the curve can be generalized to give a similar rule that holds for the alloys in question,[51] as well as for alloys between transition metals and metalloids (for example, aluminum, silicon, gallium). In all of these cases, the magnetic moment is proportional to the average magnetic valence z_M and is given by $m = z_M + 2n_{sp\uparrow}$ (described in detail in reference [48]).

Herein, the localized part of the Slater–Pauling curve, where iron and the bcc alloys are found, is of greater interest. From the definitions above, an alternative equation for the magnetic moment is easily found [Eq. (7)]. The minimum in

$$m = n_V - 2n_\downarrow \quad (7)$$

the minority DOS of the materials in this region (as for iron, Figure 11, left) constrains the number of electrons in the minority d bands to be approximately 3. By neglecting the s and p electrons, the magnetic moment for the localized part of the Slater–Pauling curve can be approximated by subtracting 6 from the average number of valence electrons per atom, according to Equation (8).

$$m \approx n_V - 6 \quad (8)$$

Half-metallic ferromagnets are expected to exhibit a real gap in the minority DOS at the Fermi energy. The existence of this gap requires that the number of occupied minority states be an integer, as is the case when $m_{HMF} = n_V - 6$.[48,52] However, in general, this rule may lead to a non-integer moment if the average number of valence electrons is a non-integer. For well-ordered compounds, it may be more practical to use the total number of valence electrons N_V per formula unit.

For $C1_b$ compounds with three atoms in the formula unit, the valence-electron rule described by Equation (9), where M

$$M_{C1b} = N_V - 18 \quad (9)$$

is the magnetic moment per formula unit, is expected. For Heusler compounds with four atoms per formula unit, the corresponding rule is given by Equation (10).

$$M_{L21} = N_V - 24 \quad (10)$$

Prominent exceptions to these rules are the conventional semiconductors and zinc-blende-type half-metals, which follow the eight-electron rule. A more chemical interpretation is also possible for the $C1_b$ (18-electron rule, as for transition-metal complexes) and Heusler (24-electron rule, see Section 3.3.2) compounds. However, other alloys often do not fulfill the symmetry requirements of the Slater–Pauling rules.

Note that the complete disorder in the $L2_1$ Heusler compounds results in an A2 (bcc) structure. Thus, the ferromagnetic Heusler compounds could be expected to behave like the alloys found on the localized part of the Slater–Pauling curve. This situation distinguishes the Heusler compounds from most of the other compounds described herein, which may also have magnetic moments that depend linearly on the valence electron concentration, but which adopt crystal structures of different symmetry.

3.3. Half-Metallic Ferromagnets

The dependence of spin polarization on temperature in half-metallic ferromagnets was recently investigated theoretically[53,54] and experimentally.[55] The magnetization of a normal ferromagnet (with a high Curie temperature) is reduced at ambient temperature. Similarly, the minority DOS of a half-metallic ferromagnets becomes nonzero at finite temperatures due to spin-rotation. A reduction of the spin polarization may also be caused by crystal disorder, interfaces, and surfaces. These findings are important for room-temperature applications of half-metallic ferromagnets: very high Curie temperatures and a high degree of order are prerequisites for a high MR.

3.3.1. Covalent Half-Metals

A possible way to produce a band gap in the overall band structure is by introducing covalence. Silicon is a semiconductor because of the strong covalent bonding between the silicon atoms; its electronic structure is shown in Figure 13. Silicon crystallizes in the diamond structure, in

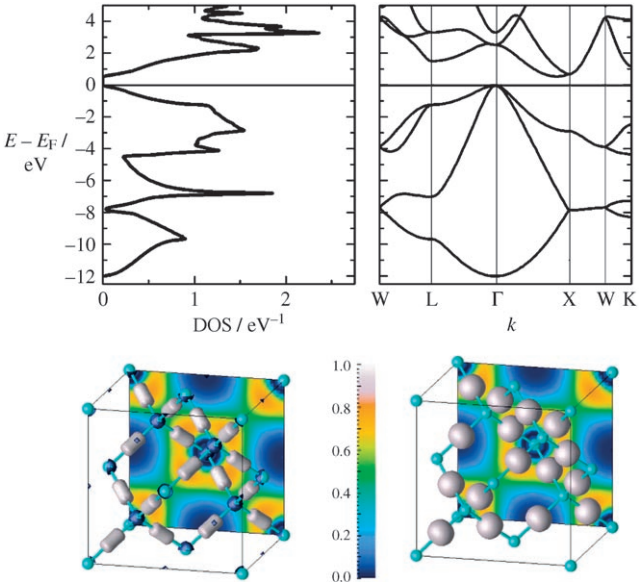

Figure 13. DOS curve (top left) and band structure (top right) for silicon. The charge density (bottom left) and electron localization (bottom right) in the crystal structure are also illustrated.

which each silicon atom is surrounded by four others. Each silicon atom is sp^3-hybridized. Four fully occupied bonding bands are separated from the unoccupied antibonding bands by a band gap. Other semiconductors, such as GaAs, crystallize in the zinc-blende (ZnS) structure. ZnS has the same number of valence electrons (8 valence electrons or, if the 10 3d electrons are included, 18 valence electrons) as these compounds and, in a first approximation, a similar band structure. All of these semiconductors exhibit a band gap in their band structures, which is identical for both spin directions and is responsible for the transport behavior of the material. For half-metals, there is a band gap in only one spin direction, which is equally important for their transport properties. This band gap prevents a spin flip, as no spin-down states are available within the gap.

3.3.2. $C1_b$ and $L2_1$ Compounds

Half-metallic ferromagnetism was first discussed for the $C1_b$ compound NiMnSb.[3] Two alternative structural descriptions of the $C1_b$ structure ($F\bar{4}3m$, sometimes falsely called half-Heusler) are possible. The common description is that the $C1_b$ compounds of composition XYZ (X, Y = transition metals, Z = main-group element) consist of three interpenetrating fcc lattices. From the viewpoint of electronic structures, the most appropriate description of these compounds is as a zinc-blende YZ lattice stuffed with X atoms (Figure 14).

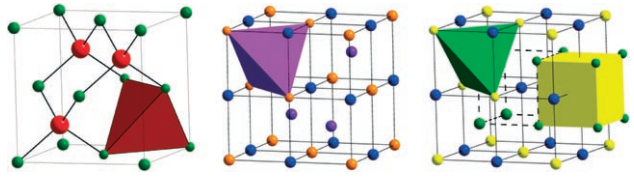

Figure 14. The zinc-blende B3 (left; YZ, Y = red, Z = green), $C1_b$ (middle; XYZ, X = violet, Y = blue, Z = orange), and Heusler $L2_1$ (right; X_2YZ, X = green, Y = blue, Z = yellow) structures.

In 1984, Kübler found that the Slater–Pauling rule is useful for describing the magnetic properties of the $C1_b$ and $L2_1$ compounds.[48,56] As an example for a half-metallic $C1_b$ compound, the electronic structure of NiMnSb is shown in Figure 15. Whangbo et al.[57] recognized that many XYZ

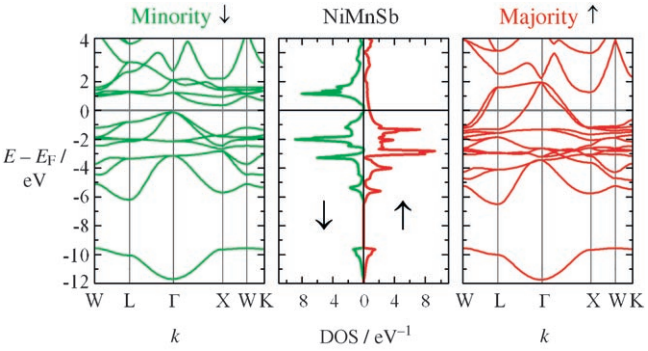

Figure 15. Spin-polarized band structure (left and right) and DOS curve (middle) for NiMnSb.

compounds can be thought of as comprising X^{n+} ions stuffed in a zinc-blende-type $[YZ]^{n-}$ sublattice, where the number of valence electrons associated with the $[YZ]^{n-}$ sublattice is 18 ($d^{10} + s^2 + p^6$). Such closed-shell 18-electron compounds are nonmagnetic and semiconducting. The prototype for a nonferromagnetic compound is CoTiSb.[58,59]

Galanakis placed the 18-electron rule for $C1_b$ compounds (with three atoms per formula unit) on a more formal footing, and discussed the basic electronic and magnetic properties of the half-metallic compounds through the analysis of ab initio band-structure calculations.[60] The origin of the gap in both the $C1_b$ and the Heusler alloys arises from d–d hybridization. For both families of compounds, the total spin magnetic moment scales with the number of valence electrons and can be described by the Slater–Pauling rule, thus opening the way for engineering new half-metallic compounds with desired magnetic properties. This behavior is governed by the fact that the number of minority valence electrons per formula unit is an integer that is given by the number of occupied minority valence bands; for the $C1_b$ compounds, nine minority valence bands contain 18 electrons.

The number of magnetic $C1_b$ compounds is smaller than the number of magnetic Heusler compounds. Most of the magnetic and half-metallic $C1_b$ compounds contain manganese or a rare earth.[61] This is not accidental because, as described by Kübler et al.,[62] the properties of the manganese ions in the Y position of the Heusler compounds must be taken into account. These manganese ions, which have an approximate Mn^{3+} configuration, have a highly localized moment that ranges from 3–4 μ_B. The rare-earth ions (RE) in $C1_b$ compounds (for example, RENiSb or REAuSn) also exhibit a charge of +3 and a magnetic moment corresponding to localized f states.[63]

Heusler compounds have the chemical formula X_2YZ (X, Y = transition metals, Z = main-group element).[64,65] Ordered Heusler compounds crystallize in the $L2_1$ structure ($Fm\bar{3}m$).[66] The additional X atom fills the remaining tetrahedral vacancy in the $C1_b$ (XYZ) structure, which changes the symmetry of the crystal structure dramatically. In the $L2_1$ structure, the two X atoms occupy sites with T_d symmetry, and the Y and Z atoms occupy sites with O_h symmetry.

In addition to the localized magnetic moment of the Y atom at the cubic site, the X atoms at the tetrahedral sites (which form a simple cubic sublattice) interact with one another, which may lead to an additional itinerant magnetic interaction between the X atoms. In the case of four atoms per formula unit, as is the case in Heusler compounds, 24 (six times the number of atoms) must be subtracted from the number of valence electrons per formula unit (s and d electrons for the transition metals, and s and p electrons for the main-group element) to obtain the magnetic moment per formula unit, according to Equation (10). This rule is strictly followed for half-metallic ferromagnets.[67,68] Whereas $C1_b$ compounds usually only exhibit a localized moment at the Y site, the magnetic interactions in Heusler compounds are more complicated, because the additional X atom results in an additional magnetic interaction. There are more $L2_1$ compounds than $C1_b$ compounds, and the probability of finding half-metallic ferromagnets among the $L2_1$ compounds is greater, because of the presence of the second magnetic sublattice.

Figure 16 shows the Slater–Pauling behavior of selected Heusler compounds with 3d transition metals at the X and Y sites.[67] The magnetic moments were obtained from full-potential gradient-corrected density functional theory (DFT) calculations. The Co_2YZ compounds strictly follow the Slater–Pauling rule [Eq. (10)], whereas for other X_2YZ compounds with iron, nickel or copper at the X site, pronounced deviations from integer moments are observed. These latter compounds are, therefore, not expected to exhibit half-metallic ferromagnetism, as was also indicated by the band-structure calculations.

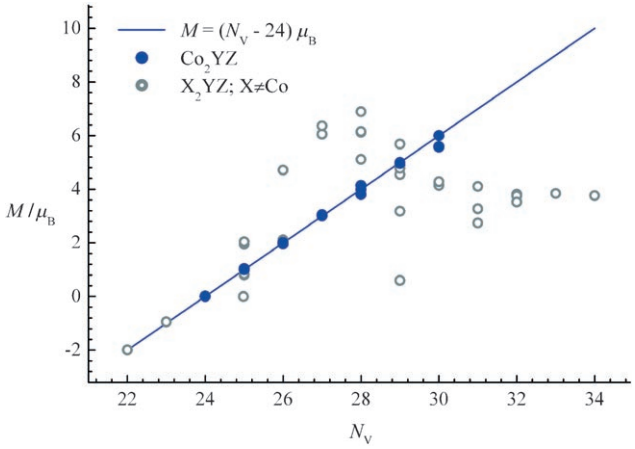

Figure 16. Comparison of the experimental magnetic moments per formula unit for selected Heusler compounds to the Slater–Pauling rule (blue line).

Plotting the Curie temperatures of the known 3d-transition-metal-based Heusler compounds as a function of their magnetic moments indicates a linear dependence (for example, the half-metallic Heusler compounds with X = Co; Figure 17[67]). According to this plot, the Curie temperature

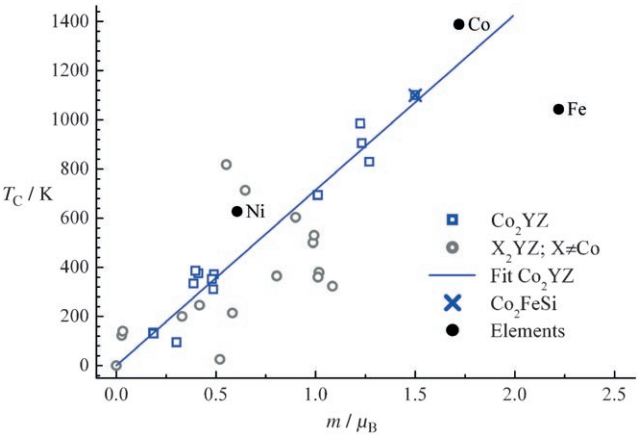

Figure 17. Plot of the Curie temperatures of iron, nickel, cobalt, and selected Heusler compounds as a function of the magnetic moment per atom. The blue line is a linear fit to the data for the Co_2YZ compounds.[71,72]

is highest for the Heusler compounds with the largest magnetic moment or, equivalently, the highest valence-electron concentrations. By extrapolating the linear dependence, T_C is estimated to be above 1100 K in compounds with moments of $6\mu_B$, that is, with 30 valence electrons per formula unit.[52,69,70] In particular, the cobalt-based compounds generally exhibit the highest Curie temperatures and the highest magnetic moments per formula unit.

3.3.3. *Ionic Half-Metals*

Small band widths in the overall electronic band structure of a solid can also lead to a band gap. Small band widths are observed in highly correlated oxides and other strongly ionic compounds. Most transition-metal oxides are insulators or semiconductors. For these compounds to become metallic, the substitution of an element must be possible. The band widths of sulfides are generally larger; therefore, half-metallic sulfides are rare.

One example of an ionic sulfide is $Co_{1-x}Fe_xS_2$. CoS_2 crystallizes in the pyrite structure and is a nearly half-metallic ferromagnet.[73,74] Half-metallic ferromagnetism is robust across the solid solution $Co_{1-x}Fe_xS_2$,[75] which has led to renewed interest in this material (Figure 18).[76] However, the low Curie temperature of $Co_{1-x}Fe_xS_2$ makes its use as a spin injector in spintronics unlikely.[76]

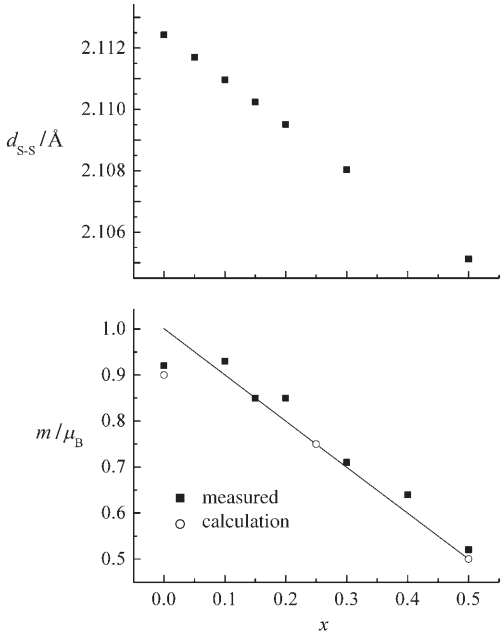

Figure 18. Half-metallic behavior in $Co_{1-x}Fe_xS_2$. A plot of the S–S bond length versus x (top) demonstrates that the minority states, which have S–S antibonding character, remain unoccupied. A plot of the experimental and calculated magnetic moment per atom versus x (bottom) is compared to the Slater–Pauling rule (line).

The perovskite manganese oxides are prominent examples of ionic half-metals.[77] The crystal structure of $LaMnO_3$ is shown in Figure 19. Stoichiometric perovskite manganites are semiconductors and often antiferromagnets. They become half-metallic by substitution. Metallic perovskite manganites such as $La_{0.83}Sr_{0.13}MnO_{2.98}$ exhibit CMR near the ferromagnetic transition temperature, as shown in Figure 20.

3.3.4. *Ferromagnetic Semiconductors*

The next step is the design of a ferromagnetic semiconductor with a Curie temperature higher than room temperature. Many attempts were made, because no such material was known until a few years ago. The advantage of ferromagnetic semiconductors as potential sources for spin-polarized electrons is their easy integration into semiconduc-

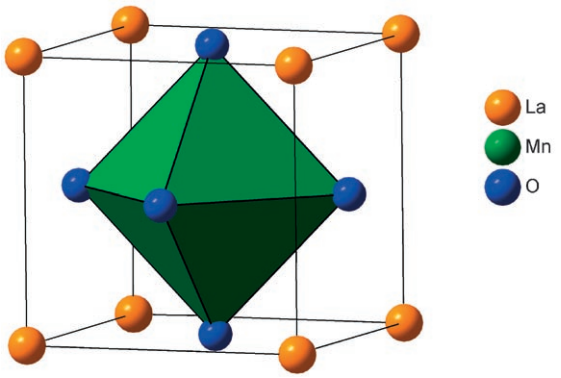

Figure 19. Structure of the perovskite $LaMnO_3$.

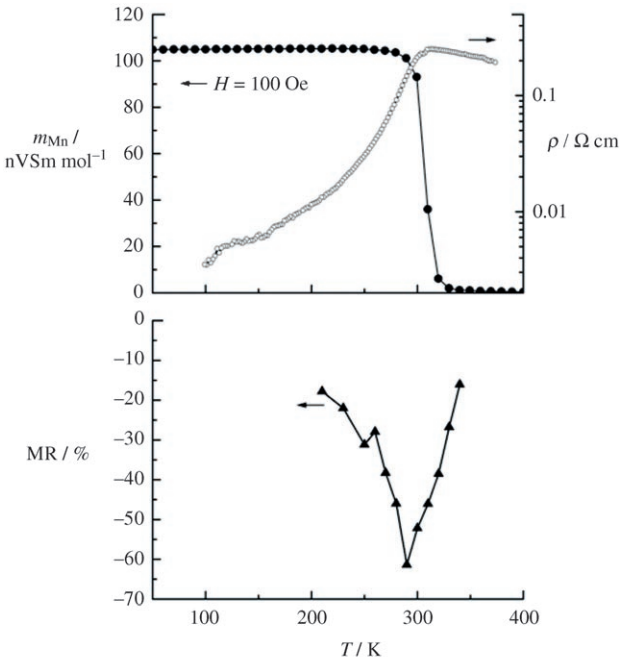

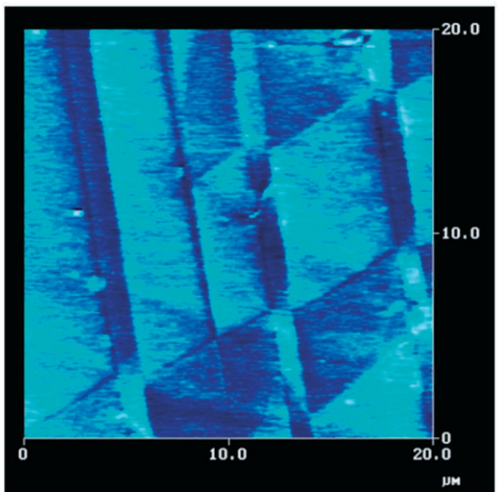

Figure 20. Temperature dependence of the magnetic moment per manganese atom (top, left axis), the resistivity (top, right axis), and the MR (middle) of a single crystal of $La_{0.83}Sr_{0.13}MnO_{2.98}$.[78] A magnetic force microscopy (MFM) image (bottom) of the magnetic microstructure of the (211) surface of the crystal.

tor devices. For this reasons, physicists have produced thin films of artificial ferromagnetic semiconductors by doping semiconductors with a small percentage of magnetic "impurities".

Herein, a distinction is made between the doped semiconductors described above, which are DMSs, and concentrated magnetic semiconductors (CMSs), for example, CrAs.[40] The introduction of local ferromagnetic moments into a diamagnetic semiconductor matrix, for example GaAs, through doping with manganese leads to a DMS. This process results in the combination of semiconducting and ferromagnetic properties. Because there is no Schottky barrier, the injection of spin-polarized electrons from a ferromagnetic semiconductor into a nonmagnetic semiconductor is easier than it is from a ferromagnetic metal or half-metal. The synthesis of DMS of the (III,Mn)–V type,[41,79,80] namely $In_{1-x}Mn_xAs$ alloys, and $In_{1-x}Mn_xAs/Ga_{1-x}Al_xSb$ heterostructures,[81] was fundamental to the technological breakthrough in the preparation of ferromagnetic semiconductors with high Curie temperatures. A MR of 290% was detected at 0.39 K and at nearly zero voltage for a DMS device.[82]

From the point of view of materials science, important and interesting results were obtained in experiments on multiphase and non-equilibrium transition-metal pnictide systems. For example, a material prepared by deposition of 3-nm MnSb islands on a GaAs matrix is characterized by an easy magnetization reversal and exhibits GMR in weak fields at room temperature (up to 880% at 1 T, and 320000% at 2 T).[83]

4. Colossal-Magnetoresistance Materials

In the Sections that follow, additional materials with properties that may be suitable for spintronics applications, namely materials exhibiting CMR, will be presented.

4.1. Perovskite Manganites

As described in Section 2.2.2, perovskite manganese oxides are the most prominent representatives of CMR materials. Perovskite manganites have been known since the pioneering work of Jonker and van Santen in 1950,[84] which established the close correlation between magnetism and electrical transport in these materials. At $x = 0.3$ in the phase diagram of $La_{1-x}Ca_xMnO_3$, the compound orders ferromagnetically, and the slope of its resistance–temperature curve simultaneously changes sign, indicating a transition from a semiconductor (negative slope; $T > T_c$) to a metal (positive slope; $T < T_c$). This influence of magnetic order on transport properties was first explained by Zener through the double-exchange (DEX) mechanism.[85] In this mechanism, electrons hop from an e_g state of a Mn^{3+} ion, via a 2p orbital of an oxygen atom, to an empty e_g state of a neighboring Mn^{4+} ion. Throughout, the electron spin is conserved spin because of Hund's rule. The alignment of neighboring spins in the ferromagnetic state can facilitate conduction by such e_g hopping. Thus, a paramagnetic–ferromagnetic transition is

accompanied by an insulator–metal transition for $La_{1-x}Ca_xMnO_3$ with $x = 0.3$.

In the 1950s, the details of the DEX mechanism were investigated by Anderson and Hasegawa,[86] and by de Gennes.[87] Goodenough examined the influence of the hybridization of the Mn 3d and O 2p orbitals on the nature of the magnetic exchange and produced a phase diagram for $La_{1-x}AE_xMnO_3$ (AE = alkaline earth).[88] The neutron diffraction investigations of Wollan and Koehler were pioneering both in their determination of the different magnetic structures in the $La_{1-x}AE_xMnO_3$ system, and in their use of neutrons as probes for magnetism in condensed matter.[89] As early as 1970, Searle and Wang discovered that magnetic fields significantly alter the resistivity–temperature curves of these perovskites by simultaneously shifting the insulator–metal transition to higher temperatures and lowering the magnitude of the resistivity, resulting in relatively large negative MR.[90] Thanks to the discovery of very large MR (now termed "colossal") in bulk samples[8] and thin films[9] of $La_{1-x}Ca_xMnO_3$ with $x = 0.3$, these perovskite manganese oxides have been the focus of considerable attention, particularly because of the manner in which the charge, spin, and lattice degrees of freedom are interrelated. Most perovskite manganites have Curie temperatures below room temperature, whereas some heavily doped perovskite manganites have Curie temperatures of $T_C \geq 350$ K. The optimally doped ferromagnetic perovskite manganite $La_{0.7}Sr_{0.3}MnO_3$ has a Curie temperature of 390 K and a rhombohedrally distorted perovskite structure. Calculations of the electronic structures of $La_{0.7}Sr_{0.3}MnO_3$[91] and $La_{0.67}Ca_{0.33}MnO_3$[92] place the Fermi levels slightly above the bottoms of the t_{2g} bands. The calculated ferromagnetic moments are consistently reported as being slightly less than the value of $3.7\,\mu_B$ expected for a half-metal. Coey therefore proposed that $La_{0.7}Sr_{0.3}MnO_3$ is a type-IIIA half-metal, for which states of both spin directions are present at the Fermi level, but are occupied by electrons with very different mobilities.[34]

However, it has now been established that perovskite manganites have half-metallic electronic structures at low temperatures.[93,94] Several methods can be used to determine the spin polarization. A MR of 1800 % at 4 K measured in the tunnel junction $La_{0.67}Sr_{0.33}MnO_3/SrTiO_3/La_{0.67}Sr_{0.33}MnO_3$ corresponds to a spin polarization of 95 %.[30] Andreev-reflection measurements on a single crystal of $La_{0.67}Sr_{0.33}MnO_3$ gave a spin polarization of 80 %.[95]

In addition to having low Curie temperatures, perovskite manganites are difficult to integrate into semiconductor microelectronic devices, owing to differences between the crystallographic parameters of the perovskites and the semiconductors. CMR in the perovskite manganese oxides has been the subject of a number of reviews.[10,77,96]

4.2. Ruddlesden–Popper Compounds

The layered compound $LaSr_2Mn_2O_7$ is an $x = 2$ member of the well-known Ruddlesden–Popper series described by the general formula $AX(ABX_3)_x$ (with A = Sr, La; B = Mn, X = O) and consists of single rock-salt layers interleaved by double perovskite layers (Figure 21).[97] This compound, which crystallizes in the space group *I*4/*mmm*, is closely related to the high-T_C superconductors $YBa_2Cu_3O_{7-x}$.[98] Like the related perovskite system $La_{1-x}Sr_xMnO_3$,[84] the layered

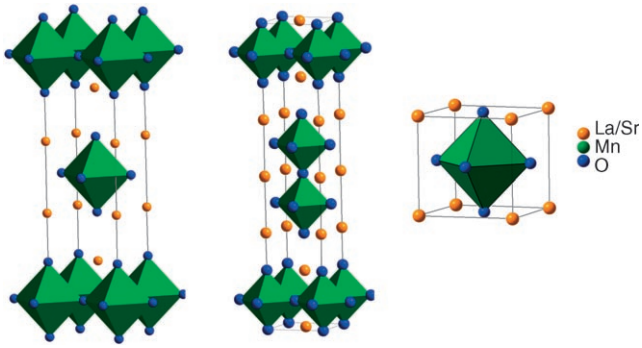

Figure 21. Structures of the $A_{x+1}B_xX_{3x+1}$ or $AX(ABX_3)_x$ Ruddlesden–Popper series (with A = Sr, La, B = Mn, X = O) for $x = 1$ (left) and $x = 2$ (middle). The perovskite structure is reached for $x = \infty$ (right).

system $La_{1+x}Sr_{2-x}Mn_2O_7$ has long been known to exhibit Zener DEX,[99,100] whereby electrons hop with spin memory.[85] As a result of the DEX mechanism, the paramagnetic–ferromagnetic transition ($T_C \approx 30$ K for $x = 0.2$) is accompanied by a transition from a semiconductor to a poor metal, and the system exhibits CMR in the low-temperature, metallic regime.[101,102] The salient features of the system are the following: ferromagnetism for $0.1 \leq x \leq 0.5$,[103] the absence of a ferromagnetic transition (and hence of a metallic phase) when lanthanum is replaced by a smaller lanthanide,[104–107] and unusual structural changes (studied for $x =$ 0.2) when the metal–insulator transition is traversed or when a smaller lanthanide is used.[108,109] In the ferromagnetic $La_{1+x}Sr_{2-x}Mn_2O_7$ compounds, the saturation value of the magnetic moment per manganese atom is usually on the order of $3\,\mu_B$, smaller than the expected spin-only value of $(3.5 + x/2)\,\mu_B$. Also of note is the complex transport behavior of the $x = 0$ compound, $LaSr_2Mn_2O_7$, which shows evidence of a real-space ordering of holes that is accompanied by a transition to an antiferromagnetic state as the temperature is lowered.[110] Furthermore, nonstoichiometric samples in this class of materials exhibit novel microstructural features.[105,106,111]

Comparison of the electronic structure of the layered manganite $LaSr_2Mn_2O_7$ to that of the oxygen-deficient cuprate $La_2CaCu_2O_6$ reveals that similar nesting motifs (Van Hove singularities) occur in the conduction bands near the Fermi levels.[112] Despite the similarities of their spin-polarized electronic structures, the Van Hove singularities occur at different electron counts, resulting in the manganite having a magnetic ground state and the cuprate a superconducting ground state. The main differences in the electronic structures arise from differences in the filling of the frontier 3d levels ($t_{2g}^3 e_g^1$ for Mn^{3+} versus $t_{2g}^6 e_g^3$ for Cu^{2+}). For both compounds, strong in-plane bonding between the metal $3d_{x^2-y^2}$ orbitals and the oxygen $2p_x$ and $2p_y$ orbitals leads to dispersive $3d_{x^2-y^2}$ bands, whose widths hide the Jahn–Teller

distortion. The metal t_{2g} bands are flat and are responsible for the local magnetic moment. In the frame of a two-band model, these bands and the Van Hove singularities contribute to the unusual properties of the compounds. As for the high-temperature superconductors, a Van Hove singularity occurs near the Fermi level in the electronic structure of $LaSr_2Mn_2O_7$.[112]

Such features can be easily visualized by determining the Fermi surface (the three-dimensional electronic structure at the Fermi energy). By using angle-resolved photoemission spectroscopy, Mannella et al. recently investigated the electronic structure of the layered Ruddlesden–Popper manganites, and the experimental results were in good agreement with theoretical predictions.[113]

4.3. The Pyrochlore $Tl_2Mn_2O_7$

$Tl_2Mn_2O_7$ is a ferromagnetic compound with the pyrochlore structure ($A_2B_2O_7$): thallium atoms occupy the A site, which is coordinated by eight oxygen atoms in a strongly distorted cubic arrangement, and manganese atoms occupy the octahedral B site. The AO_8 cubes and the BO_6 octahedra are linked to form a three-dimensional network. The thallium ions are formally trivalent and the manganese ions formally tetravalent.

The electronic structure of $Tl_2Mn_2O_7$ calculated by Singh supports the view of CMR presented herein.[114] One might expect the electronic structure of the pyrochlore to be quite different from those of the perovskite manganese oxides, particularly since the Mn-O-Mn connectivities are very different in the two structures. From the atom and orbital projections (not shown) of the calculated DOS (Figure 22), it is apparent that the three 3d electrons of the Mn^{4+} ions completely fill the t_{2g} levels, as a result of complete spin polarization. The manganese 3d states are not very disperse, since the pyrochlore topology does not allow bonding interactions to propagate very far. At the Fermi energy, there is a small total DOS arising from Tl–O bonding states. $Tl_2Mn_2O_7$ is a ferromagnetic semimetal with approximately 0.01 electrons and holes per formula unit. This semimetallic

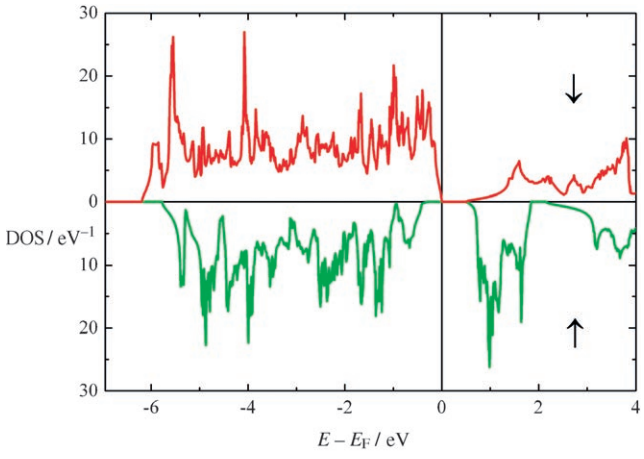

Figure 22. Spin-polarized DOS curve for $Tl_2Mn_2O_7$.

behavior originates from the small amount of heavy holes (which have a large effective mass because of the small positive curvature of the conduction band at the Γ point) at the edge of the narrow majority band with manganese t_{2g} character and the same number of conduction electrons in a broad minority band with thallium 6s, oxygen 2p, and manganese 3d character. This situation is not unusual for Tl^{3+} compounds: Tl_2O_3 itself is a semiconductor without a band gap, because of the overlap of empty thallium 6s and 6p states with filled oxygen 2p states. In the thallium cuprate superconductors, thallium states also participate in the conduction mechanism.[115]

4.4. Copper-Containing Compounds

Zeng et al. have synthesized a number of perovskites containing copper and manganese, $CaCu_{3-x}Mn_{4+x}O_{12}$ ($0 \le x \le 3$).[116] The highest MR values were found for the sodium-doped compound $Ca_{0.5}Na_{0.5}Cu_{2.5}Mn_{4.5}O_{12}$ (−32%) and for $CaCu_{2.5}Mn_{4.5}O_{12}$ (−28%) at 4.2 K and 5 T. However, the mechanism of MR in these compounds must be different from that in the simple perovskite manganites. In this case, the MR does not occur at the semiconductor–metal transition and decreases smoothly with increasing temperature or x. The MR of these copper-containing compounds is highly sensitive to low applied magnetic fields and has good temperature stability.[116]

In 1997, a CMR of 20% was found for the chromium-based chalcogenide spinels $Fe_{1-x}Cu_xCr_2S_4$ at 180 K. This was the first report of large MR in compounds not containing heterovalent distortion-inducing ions, manganese, or oxygen, and not adopting a perovskite structure.[15] These CMR compounds are the electronic counterparts of superconducting $CuRh_2S_4$.[117]

Most CMR compounds with the spinel structure, however, have a transition temperature below room temperature. The Curie temperatures of the semiconductors $CuCr_2Se_{4-x}Br_x$ exceed room temperature, but these materials are unstable in air. The multicomponent semiconductor solid solutions based on the ferromagnet $CuCr_2S_4$ ($T_C = 367$ K), the antiferromagnet $Cu_{0.5}E_{0.5}Cr_2S_4$ (E = In, Ga, Al), and the ferrimagnets $CoCr_2S_4$ and $MnCr_2S_4$, which exhibit ferromagnetism above room temperature, are also of interest.[118] Although these solid solutions retain some of the properties of the ferromagnetic matrix $CuCr_2S_4$ and exhibit p-type conductivity, they are still far from meeting the purity requirements for electronic materials.

4.5. The Rare-Earth Compounds GdI_2, Gd_3S_4, EuS, and EuO

GdI_2 was examined during a systematic search for magnetic analogues of superconductors.[18] GdI_2 is a layered d^1 compound that is isostructural with and nominally isoelectronic to the hexagonal superconductors 2H-TaS_2 and 2H-$NbSe_2$. Its crystal structure is shown in Figure 23. GdI_2 crystallizes in the hexagonal 2H-MoS_2 structure and comprises close-packed layers of metal atoms sandwiched by

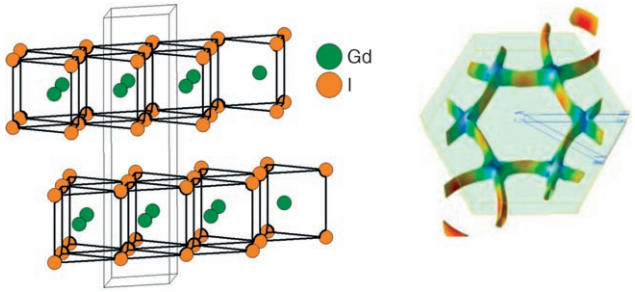

Figure 23. Crystal structure (left) and Fermi surface (right) of GdI_2.

layers of iodine atoms, which together form GdI_2 slabs. In addition to the half-filled 4f shell of the Gd^{3+} ions, an extra electron is delocalized in the gadolinium 5d conduction band and is involved in Gd–Gd bonding. The calculated spin-polarized electronic structure indicates a nearly full polarization of the $5d_{z^2}$ conduction electrons.[18] The Fermi surface of GdI_2 is also shown in Figure 23. The compound undergoes a ferromagnetic transition near 300 K,[119] as a result of the half-filled 4f band. Because of the trends observed for the layered Ruddlesden–Popper manganites and cuprates (Section 4.2), GdI_2 was investigated for CMR. Indeed, CMR of significant magnitude, approximately 70% at 7 T and close to room temperature, was found for GdI_2 (Figure 24).[18]

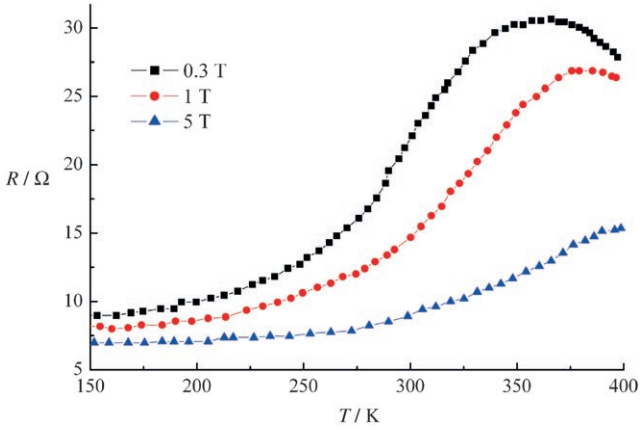

Figure 24. Temperature and field dependence of the resistance of GdI_2.

According to the theoretical study by Eremin et al.,[120] the MR of for GdI_2 is due to strong spin-disorder scattering of the 5d conduction electrons by the localized 4f electrons. This hypothesis is largely in agreement with the two-band model. Recently, band-structure calculations showed that the semiconductor–metal transition at the Curie temperature can be explained through correlation effects.[121] In addition, the electronic structure exhibits a Van Hove singularity slightly below the Fermi level. This feature led to the prediction that enhanced CMR could be achieved by electron doping of GdI_2, for example, with hydrogen.[18]

To verify this prediction, Ryazanov et al. prepared and studied a series of hydrogen-doped samples of composition GdI_2H_x over the entire homogeneity range ($0 \le x \le 1$).[122] Initial studies of samples with $0.28 \le x \le 0.34$ indicated that hydrogen insertion into GdI_2 results in a suppression of the ferromagnetic order and the thermally activated conduction.[120] The system goes from a ferromagnetic state to a spin-glass-like state at a critical hydrogen content of $x \approx 1/3$ (Figure 25). When approaching $x = 1/3$, there is a sharp

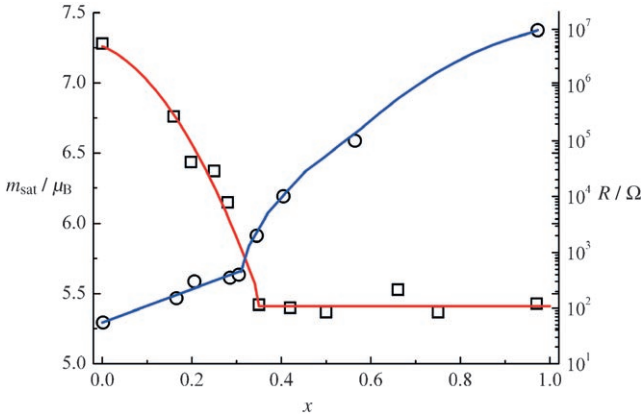

Figure 25. Dependence of the saturation moment at 5 K (□) and the resistance at room temperature (○) of GdI_2H_x on x. The lines are guides for the eye.

change in the activation energy, as well as in other macroscopic parameters.[120] In agreement with the prediction, a large MR of approximately 95% was observed for ferromagnetic GdI_2H_x samples with $x = 0.24$ and 0.26 near the magnetic transition at $T_C \approx 170$ K in a field of 7 T (Figure 26). These

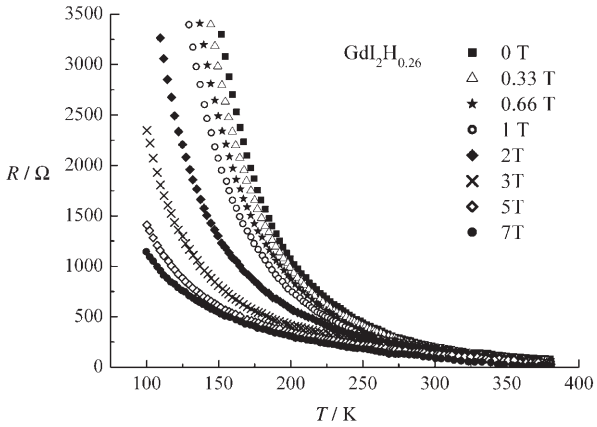

Figure 26. Temperature and field dependence of the resistance of $GdI_2H_{0.26}$.

layered compounds exhibit thermally activated conductivity, which is associated with a gradual increase in the activation energy below the transition temperature. The MR is already remarkably large at room temperature (ca. 50% at 7 T), and increases continuously with decreasing temperature, reaching saturation in the ferromagnetic range.[122] Magnetic studies revealed the presence of competing ferromagnetic and antiferromagnetic interactions, which result in spin freezing at low temperatures. These results agree with earlier investigations, which indicated that the large MR is governed by

the spin disorder in the system. The resistance is substantially suppressed when strong magnetic fields are applied, which implies that the charge-carrier transport in the ferromagnetic range is mainly mediated by a variable-range hopping mechanism. However, GdI_2 compounds, including those doped with hydrogen, are very sensitive to air and, therefore, not suitable for applications.

In the europium chalcogenides EuX (X = O, S, Se, Te), the internal magnetic field of the Eu^{2+} ions produces a giant Zeeman splitting of the spin sub-bands (ca. 0.5 eV for EuS).[123,124] Because of this effect, these magnetic insulators are efficient spin filters in metal–magnet or insulator–metal heterostructures.[125] EuO is optically transparent and, as a ferromagnetic insulator, is an attractive material for magneto-optical applications. In addition, doping with other rare earths or an excess of europium leads to a field-dependent insulator–metal transition and to CMR with a resistivity change of several orders of magnitude.[18,126] EuO may be grown epitaxially on silicon for the injection of spin-polarized charge carriers into semiconductors and is, therefore, promising for spintronics applications.[127] EuO also exhibits a large Faraday rotation and may, thus, be useful in a variety of integrated magneto-optical and electro-optical systems, especially those that require cooling with liquid nitrogen. For thin films of gadolinium-doped EuO, the Curie temperature ranges from 69 K for stoichiometric EuO to approximately 170 K for a film with an optimal doping of approximately 4%.[128] The magnetic moments of the gadolinium and europium ions couple ferromagnetically.[128]

In 1983, von Molnar et al. observed CMR for $Eu_{1-x}Gd_xSe$ with a resistivity change of $10^5\ \Omega$cm in a field of 1.5 T.[20] In addition, Gd_3S_4 exhibits an insulator–metal transition near the Curie temperature, which can be suppressed by an external magnetic field. This behavior is not accidental, as the electronic structures of both EuO and Gd_3S_4 exhibit Van Hove singularities at the Fermi levels.[20] Earlier studies of valence instabilities in europium compounds led to the conclusion that there is a relationship between superconductivity, valence fluctuations, and CMR.[129] Of the compounds adopting the cubic Th_3P_4 structure, superconductivity is observed for La_3S_4 ($T_C = 8$ K),[130] inhomogeneous mixed-valence is found in Eu_3S_4,[131] and a large negative MR is observed for $Gd_{3-x}S_4$.[20] However, the Curie temperatures of the rare-earth chalcogenides are far below room temperature, limiting the applications of these compounds.

4.6. Zintl Compounds

Zintl compounds are named after Eduard Zintl, who recognized that intermetallic compounds follow electron-counting rules under certain conditions. These compounds are not really metallic, and a bonding description must include ionic and covalent interactions. This class of spintronics materials is, therefore, located between the ionic and covalent half-metals.

Kauzlarich et al. synthesized several Zintl compounds containing europium and manganese that exhibit large MR.[22,23,132] $EuIn_2P_2$ crystallizes in the hexagonal space group $P6_3/mmc$, and contains alternating layers of composition Eu^{2+} and $[In_2P_2]^{2-}$.[133] This compound is paramagnetic at high temperatures and undergoes a magnetic transition at 24 K. The temperature-dependence of the resistivity of this compound suggests interactions between the conduction electrons and localized spins. Negative CMR of up to 398% is observed at 5 T and 24 K. Another related semiconducting Zintl compound is $Eu_3In_2P_4$, which exhibits a negative MR of 30% at 2 K in an induction field of 5 T. A fit of high-temperature susceptibility data gave a positive Weiss constant, which suggests ferromagnetism, while the shape of the susceptibility–temperature curve at low temperatures suggests antiferromagnetism.[22]

$Ca_{14}MnSb_{11}$ crystallizes in the tetragonal space group $I4_1/acd$ and also exhibits large negative MR. The calculated electronic structures of the manganese-containing "14-1-11" compounds are very close to half-metallic.[23] The magnetic moment of the manganese-based compounds is $4\mu_B$. A hole resides in the $MnSb_4$ tetrahedral units and partially compensates the moment of the high-spin $3d^5$ manganese ions.

The transition-metal Zintl phases $Ca_{14-x}Eu_xMnSb_{11}$ ($0 \le x \le 14$) are isostructural with $Ca_{14}MnSb_{11}$ (Figure 27). In $Eu_{14}MnSb_{11}$, the manganese moments interact ferrimagnetically with the Eu^{2+} ($4f^7$) moments. The paramagnetic Curie temperature of the $Ca_{14-x}Eu_xMnSb_{11}$ compounds shows an interesting variation with x, and the easy axis of magnetization gradually changes from perpendicular (for $Ca_{14}MnSb_{11}$, $x = 0$) to parallel (for $Eu_{14}MnSb_{11}$, $x = 1$) to the c axis.[22] The band structures of the compounds in the ferromagnetic state are nearly half-metallic.

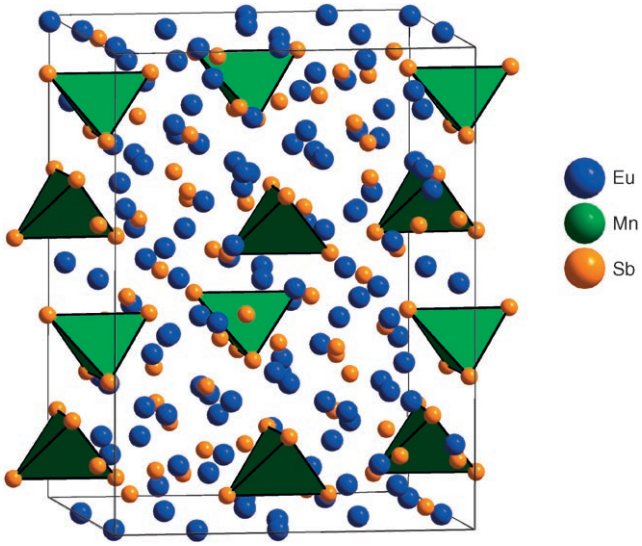

Figure 27. Structure of the Zintl compound $Eu_{14}MnSb_{11}$.

5. Ferromagnetic Semiconductors for Spintronics

5.1. Transition-Metal Oxides

Transition-metal oxides are usually antiferromagnetic insulators or semiconductors, for example, the brownmiller-

ites ($A_2B_2O_5$, A, B = metals); a few belong to the class of ferromagnetic semiconductors, the CMSs.[133] There is a general interest in ferromagnetic semiconductors and semimetals because these compounds have a larger spin-flip length, which is favorable for laterally patterned spin devices. The first ferromagnetic semiconductor, $CrBr_3$ ($T_C = 37$ K), was synthesized in 1960.[133] The few known ferromagnetic oxides have relatively low Curie temperatures: $BiMnO_3$ ($T_C = 105$ K),[134] $GeCuO_3$ ($T_C = 26$ K),[135] and $YTiO_3$ ($T_C = 29$ K).[136] Transition-metal and rare-earth oxides, fluorides, and phosphides are poorly compatible with semiconductor technology. Differences between the crystal structures of conventional semiconductors, such as GaAs and silicon, and the CMSs prevent the latter from being integrated into semiconductor heterostructures for spintronics applications. The properties of the CMSs and other semimetals are briefly outlined in reference [137]. Finding ferromagnetic semiconducting oxides remains a challenge for solid-state chemists.

5.2. GaAs and GaN Doped with Manganese

The detection of ferromagnetism in II–VI DMSs and oxides inspired a great deal of research interest. Major progress in this area was achieved by Awshalom et al., who demonstrated that electrons can retain their spin polarization over unexpectedly long times and distances.[42,46,47] Magnetic semiconductors can be formed by doping III–V compounds with manganese;[45] however, these doped compounds exhibit transition temperatures of only 150 K. The main challenge for practical applications of DMS materials is the attainment of Curie temperatures higher than room temperature to allow compatibility with junction temperatures. According to predictions based on mean-field theory, conventional III–V and II–VI semiconductors doped with transition metals are promising candidates for DMS materials with Curie temperatures above room temperature. Transition-metal-doped ZnO and GaN have been the most extensively studied materials.[138] The prerequisites for magnetic ordering in such materials are a transition-metal doping of at least 5% and an additional hole doping; the holes mediate the exchange interactions responsible for the magnetic ordering. An additional advantage of DMSs based on ZnO and GaN is that they can be readily incorporated into existing semiconductor heterostructures. A number of optical and electronic devices have already been realized. The exploration of the underlying physical properties allows applications based on new combinations of quantum structures and magnetism in semiconductors.

5.3. Transparent Oxides Doped with Ferromagnets

New candidates for ferromagnetic semiconductors have recently been synthesized by doping semiconducting transition-metal oxides with magnetic impurities. Some of these materials exhibit ferromagnetism at room temperature and above. The critical issue is the origin of this behavior. In many cases, complex solid-state chemistry is involved in the synthesis and determines the properties of the resulting material. To accurately identify the origin of the magnetism, the observation of room-temperature ferromagnetism must be accompanied by a careful identification of the phases and structures that are present in the material.[139] Clusters of metallic cobalt, for example, can lead to ferromagnetism above room temperature, but are not expected to be half-metallic. The observation of transition temperatures above 300 K for cobalt-substituted TiO_2[140] and other materials can probably be attributed to sample inhomogeneities.[141] On the basis of theoretical calculations, ZnO was identified as a particularly promising candidate for yielding a suitable ferromagnetic semiconductor with doping. As ZnO is a semiconductor with a wide band gap (3.3 eV), a ferromagnetic version could be used as for the construction of magneto-optical devices. ZnO substituted with 5% manganese was predicted to order ferromagnetically above 300 K,[138] and the ground state for ZnO substituted with other transition metals was also predicted to be ferromagnetic;[142] however, a simultaneous hole (p-type) doping is necessary.[143] To confirm the predictions, a number of experiments have been performed on ZnO substituted with manganese[144–146] and with other transition metals[146–149] Several measurements on thin films of cobalt- and manganese-substituted ZnO suggest ferromagnetic behavior, but other measurements give no indication of a magnetic transition. One hypothesis is that a clustering of the magnetic ions could be responsible for the observed ferromagnetic behavior.[150] Recently, room-temperature ferromagnetism was also observed for bulk manganese-doped ZnO prepared at low temperatures.[151] Ferromagnetism has also been observed for semiconducting quantum dots of cobalt-doped ZnO,[152] but the magnetic properties of nanoparticles can differ from those of the bulk material.[153]

Lawes et al. discuss the properties of semiconducting bulk ZnO doped with small amounts of manganese or cobalt ($Zn_{1-x}M_xO$; M = Mn, Co; $0.02 \le x \le 0.15$).[154] The magnetic properties were investigated at temperatures as low as 2 K, but no evidence of magnetic ordering was found. Thus, the ferromagnetism of the doped bulk samples and the thin films is still under debate.[155,156] The extent to which metastable phases are accessible through special preparation techniques, such as soft chemistry ("chimie douce"), or through the synthesis of nanoparticles or thin films remains to be clarified. The importance of an additional hole doping must also be elucidated.

Research in this field is still very active. Recently, ferromagnetism was observed for CuO doped with 3.5 to 15% manganese ($T_C = 80$ K).[157]

5.4. Magnetic B3 and B4 Compounds

However, the best choice for a new spintronics material would be a ferromagnetic semiconductor (a CMS) with the zinc-blende (B3) or wurtzite (B4) structure. Such a material could be integrated into existing semiconductor technology, because both the crystal structure and the band structure could be matched with those of conventional semiconductors.

Unfortunately, only a few binary compounds of magnetic elements crystallize in the zinc-blende or wurtzite structures.

Very recently, CrAs and CrSe in the zinc-blende and wurtzite structures were proposed to be half-metallic ferromagnets.[158] Akinaga et al. succeeded in growing thin films of CrAs by using molecular beam epitaxy. They found that the CrAs films, which they assumed to adopt the zinc-blende structure, are ferromagnetic at room temperature ($T_C >$ 400 K), with a saturation moment of $3\mu_B$.[158] Bulk CrAs adopts the MnP structure and exhibits complex magnetic behavior below a transition temperature of 256 K. Bulk samples may also crystallize as Cr_2As, which is an antiferromagnet with a Néel temperature of 393 K. In good agreement with experiment, spin-polarized band-structure calculations demonstrated that ferromagnetic zinc-blende CrAs should be a half-metal with a magnetic moment of $3\mu_B$.[159] Using a simple electron-counting scheme based on the Slater–Pauling rule or the eight-electron rule, the saturation moment is estimated to be $3\mu_B$ for the half-metallic state. In a stoichiometric compound, the number of electrons per formula unit, $N_V = N_\uparrow + N_\downarrow$, is an integer. Because of the gap in one of the spin-polarized bands, $N_\downarrow$ or $N_\uparrow$ is also an integer. It follows that $N_\uparrow$ or $N_\downarrow$ and, thus, the magnetic moment per formula unit, $M = N_\uparrow - N_\downarrow$, are also integers.[34] CrAs has 11 valence electrons and is thus expected to have a saturation magnetization of $3\mu_B$ as a half-metal with the zinc-blende structure (the difference between 11 valence electrons and 8 electrons for the fully occupied bonding bands).[160] From a chemical point of view, the description of CrAs as consisting of $3d^3$ Cr^{3+} and As^{3-} ions is also plausible. The electronic structure of CrAs with the zinc-blende crystal structure corresponds to that of a half-metallic ferromagnet (Figure 28).

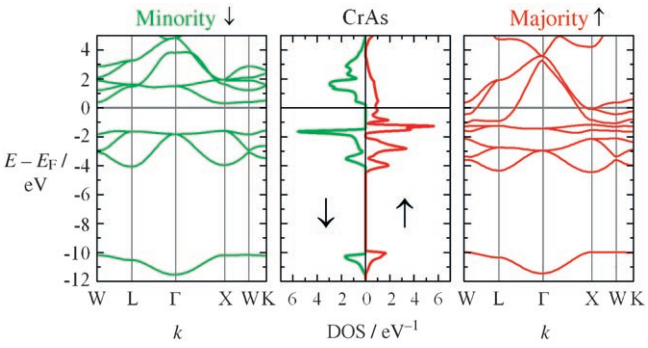

Figure 28. Spin-polarized band structure (left and right) and DOS curve (middle) for zinc-blende-type CrAs.

5.5. Doped Semiconducting $C1_b$ Compounds: $CoTi_{1-x}Fe_xSb$

As expected on the basis of the Slater–Pauling rule, the 18-electron $C1_b$ compound CoTiSb is not ferromagnetic, but rather, is a semiconductor with a gap at the Fermi energy for both spin directions. Partial replacement of titanium by iron (less than 10%) in a random manner converts the semiconductor into a half-metallic ferromagnet: in the calculated electronic structure, the DOS for one spin direction is clearly greater than zero. Measurements indicate that the resistance of pure CoTiSb decreases with increasing temperature, consistent with semiconducting behavior. In contrast, the resistance of $CoTi_{0.95}Fe_{0.05}Sb$ increases with increasing temperature, as is typical for a metal. Another important result of the calculations is that only iron atoms in the titanium position contribute to the total magnetic moment of the compound; iron atoms in the cobalt positions or in tetrahedral holes do not. The calculated value of the magnetic moment per iron atom in the titanium position changes slightly with the iron concentration, from 3.4 (5%) to $3.7\mu_B$ (10%).

The $C1_b$ structure is retained when up to 10% iron is substituted for titanium in CoTiSb. Such samples exhibit ferromagnetism and have Curie temperatures above 700 K. By carefully comparing the powder X-ray diffraction patterns of the iron-doped compounds with those of pure CoTiSb, it was determined that the iron atoms occupy the titanium position, but no other sites in the structure. For doping of up to 10% iron, no additional reflections were detected in the diffraction patterns, confirming that the structure remains the same as that of CoTiSb, that is, the $C1_b$ structure.

The Mössbauer spectra recorded for powder samples of $CoTi_{1-x}Fe_xSb$ comprise a low-intensity paramagnetic singlet and a more intense magnetic sextet. In accordance with electronic-structure calculations, the ferromagnetic subspectrum can be assigned to the presence of iron atoms in the titanium position of CoTiSb with the $C1_b$ structure. The low-intensity, nonmagnetic singlet corresponds to iron atoms in voids or in the cobalt position. On the whole, Mössbauer spectroscopy indicates that the iron atoms mainly occupy the titanium site of CoTiSb, rather than forming a separate iron phase.

The predictions of the band-structure calculations with respect to the magnetic properties of $CoTi_{1-x}Fe_xSb$ were confirmed by superconducting quantum interference device (SQUID) magnetometry and X-ray absorption spectroscopy (XAS). In general, measurements on the SQUID magnetometer allow the saturation magnetization to be determined, whereas XAS measurements with circularly polarized light (X-ray magnetic circular dichroism (XMCD)) allows the local components of the total magnetic moment to be determined. In agreement with theoretical predictions, an XMCD signal was only detectable at the Fe $L_{2/3}$ edge.

In Figure 29, the results of the magnetic studies on $CoTi_{1-x}Fe_xSb$ are summarized and compared to theoretical predictions (note that, whereas the measurements and calculations give the total magnetic moment including the orbital contribution, estimates based on the Slater–Pauling rule correspond to the spin-only magnetic moment). The hysteresis curves of the samples containing 1–10% iron indicate that $CoTi_{1-x}Fe_xSb$ is a soft magnetic material. As expected, the alloy with the highest iron concentration has the highest magnetic moment. The Curie temperature of the alloy is higher than 700 K, the temperature at which $CoTi_{0.9}Fe_{0.1}Sb$ decomposes.

Very recently, bulk-sensitive high-energy X-ray photoemission spectroscopy (HXPS) has been used to investigate the valence band of CoTiSb.[241] The sample was excited by photons with an energy of 2.5 keV. The high kinetic energy of

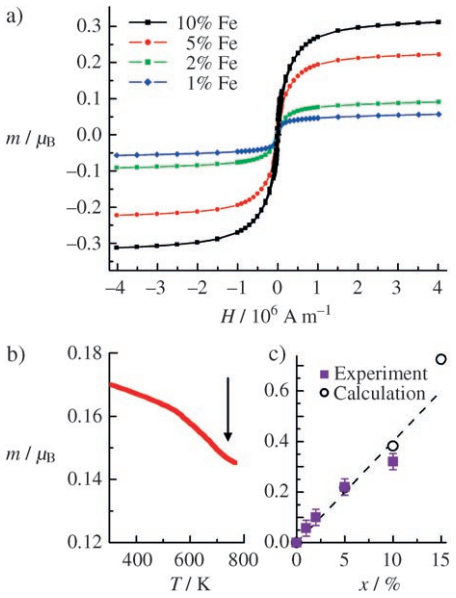

Figure 29. Magnetic properties of $CoTi_{1-x}Fe_xSb$. a) Field dependence of the magnetic moment per atom of $CoTi_{1-x}Fe_xSb$ ($x = 0.01$, 0.02, 0.05, and 0.1) at 5 K. b) Temperature dependence of the magnetic moment per atom of $CoTi_{0.9}Fe_{0.1}Sb$ at 0.1 T; the arrow indicates the onset of sample decomposition. c) Comparison of the experimental and calculated magnetic moments per atom to the Slater–Pauling rule (-----).

the electrons emitted from the valence band resulted in an escape depth of approximately 50 Å, which corresponds to approximately ten cubic cells.

The results of HXPS on CoTiSb are shown in Figure 30, where they are compared to the total DOS curve weighted by the partial photoionization cross sections. For better comparison, the weighted DOS curve was broadened by a Gaussian function with a width of 250 meV to roughly account for the experimental resolution. The high-energy spectrum reveals the low-lying s states at −11 to −9 eV below the Fermi energy, in agreement with the calculated DOS. These low-lying bands are separated from the high-lying d states by a hybridization gap typical of $C1_b$ compounds, which is clearly resolved in

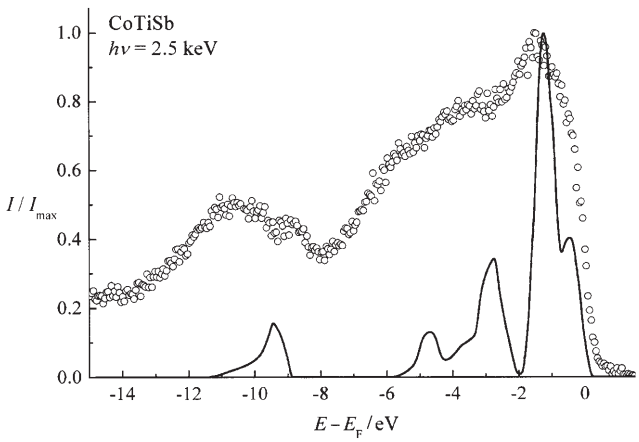

Figure 30. Comparison of the valence-band HXPS spectrum (○; excitation energy of 2.5 keV) and the weighted DOS curve (——) for CoTiSb.

both the spectrum and the calculated DOS. This gap is typically on the order of 4 eV in antimony-containing compounds. In the energy range of the d states, the spectrum agrees roughly with the shape of the total DOS curve, although the peaks in the DOS at −5 and −3 eV are not well resolved. Overall, the emission from the d states covers a larger energy range than the corresponding DOS, and the main peak at −1.5 eV in the spectrum is found at a slightly higher energy in the DOS, which implies an underestimation of correlation effects in the local-density approximation (LDA; see Section 6.5). However, the lifetime broadening and resolution of the experimental spectrum must also be considered in this comparison. At an excitation energy of 2.5 keV, the emission is still dominated by the d states of highest density at approximately −1.5 eV. Overall, the experimental photoelectron spectrum agrees with the calculated DOS. The small differences noted in the peak positions are due to the incomplete treatment of correlation effects in the LDA applied in the calculation of the electronic structure.

6. Half-Metallic Ferromagnets

CrO_2, and many double perovskites, $C1_b$ compounds, and Heusler compounds are half-metallic ferromagnets, but most of these compounds do not exhibit CMR. Although large MR were found in tunneling experiments for many of these compounds, only a few exhibit a high spin polarization in photoemission experiments. However, a high spin polarization is a prerequisite for both CMR and spin-polarized tunneling.

Coey et al. have proposed a broad classification scheme for half-metallic ferromagnets,[34] which is presented in Table 1. A material exhibiting metallic conductivity and an integer spin-only moment at $T = 0$ is a good candidate for a type-I half-metallic ferromagnet. However, the criterion of an integer spin-only moment for stoichiometric compounds (or a modified criterion for solid solutions) is a necessary, but not a sufficient condition for half-metallicity.

Type-I_A half-metals are metallic with respect to the majority electrons, but semiconducting with respect to the minority electrons; the opposite is true for the type-I_B half-metals. Half-metallic transition-metal oxides in which the 4s states of the first-row transition metal are pushed above the Fermi level are of type I_A when they have less than five 3d electrons, but are of type I_B when they have more than five 3d electrons. In half-metallic Heusler alloys containing first-row transition metals and heavy main-group elements, such as antimony, the transition-metal 3d levels are lowered below the 4s band edge due to hybridization. Examples of type-I_A half-metals are CrO_2 and Mn_2VAl, and examples of type I_B half-metals are Sr_2FeMoO_6 and Co_2MnSi.

In a second class of half-metals, designated as type II, the carriers at the Fermi level are in a band that is sufficiently narrow for them to be considered as localized. The magnetic mineral magnetite (Fe_3O_4) is a half-metal with a band gap in the majority DOS, and localized states in the minority band;[161] it is a type-II_B half-metal. A third class of half-metals (type III), known as "transport half-metals", has

Table 1: Classification of half-metallic ferromagnets.[34]

Type	DOS curve	Conduction	↑ Electrons at E_F	↓ Electrons at E_F
I_A	half-metal	metallic	itinerant	none
I_B	half-metal	metallic	none	itinerant
II_A	half-metal	nonmetallic	localized	none
II_B	half-metal	nonmetallic	none	localized
III_A	metal	metallic	itinerant	localized
III_B	metal	metallic	localized	itinerant
IV_A	semimetal	metallic	itinerant	localized
IV_B	semimetal	metallic	localized	itinerant
V_A	semiconductor	semiconducting	few, itinerant	none
V_B	semiconductor	semiconducting	none	few, itinerant

localized majority states and delocalized minority states, or vice versa.[91] The DOS at the Fermi level does not vanish for either spin direction, but the charge carriers in one spin direction have a much larger effective mass than those in the other. With respect to electronic transport, only one type of charge carrier contributes significantly to conduction. $La_{0.7}Sr_{0.3}MnO_3$ is a type-III_A half-metal; in its electronic structure, a finite DOS is present at the Fermi level for both spin directions, but the two types of charge carrier have very different mobilities. However, the question remains as to whether the low DOS near the Fermi level is related to the accuracy of the band-structure calculations and would disappear if electron–electron correlation were included.

$Tl_2Mn_2O_7$, a ferromagnetic pyrochlore, has an unusual semimetallic band structure, with approximately 0.01 electrons and holes per formula unit.[114] A small number of heavy holes are located at the top of a narrow majority band of manganese t_{2g} character, and an equal number of conductions electrons occupy a broad minority band of mixed thallium 6s, oxygen 2p, and manganese 3d character, making $Tl_2Mn_2O_7$ a type-IV_A half-metal. DMSs are included in the table as type-V half-metals.

6.1. Double Perovskites

In 1998, Kobayashi et al. discovered large MR in Sr_2FeMoO_6.[35] This material belongs to the family of double perovskites, which have the general formula $A_2BB'O_6$ (A = alkaline earth; B, B′ = transition metals). The cubic crystal structure of Ba_2FeReO_6 is shown in Figure 31 (some of the double perovskites, including Sr_2FeMoO_6, adopt distorted structures).

The half-metallic double perovskites that exhibit MR at room temperature are more promising for spintronics applications than the $AEMnO_3$ (AE = alkaline earth) perovskites. For example, the Curie temperature of Sr_2FeMoO_6 is 420 K,[35] and that of Sr_2CrReO_6 is 635 K.[162] Films of Sr_2CrReO_6 prepared by magnetron sputtering on $SrTiO_3$ substrates exhibit a transition temperature of 620 K.[163] A homogeneous polycrystalline sample of Sr_2FeMoO_6 (T_C = 416 K) exhibits a MR of 45% at 5 K and 9 T, and a MR of 6.5% at room temperature and 0.3 T.[164] In Figure 32, typical resistivity–field and hysteresis curves for Sr_2FeMoO_6 are shown. Upon doping with aluminum, the MR of $Sr_2Fe_{1-x}AlMoO_6$ increases to nearly 60% for $x = 0.15$ at 5 K and 1 T, and the electronic transport properties improve.[165]

Several other doping experiments were performed to understand the complex magnetic behavior of these ferrimagnetic materials with two magnetic sublattices.[166,167] Strong correlations between the electronic, structural, and magnetic properties were found in studies of the doped double perovskites $Sr_2Fe_{1-x}M_xReO_6$ (M = Zn, Cr; $0 \le x \le 1$). The interplay between the Van Hove singularity and the Fermi level plays a crucial role in determining the magnetic properties.

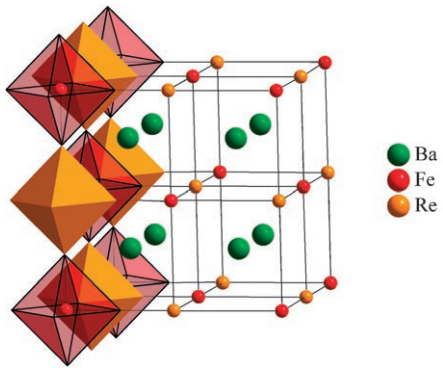

Figure 31. Structure of the double perovskite Ba_2FeReO_6. For clarity, only one layer of corner-sharing FeO_6 and ReO_6 octahedra is shown.

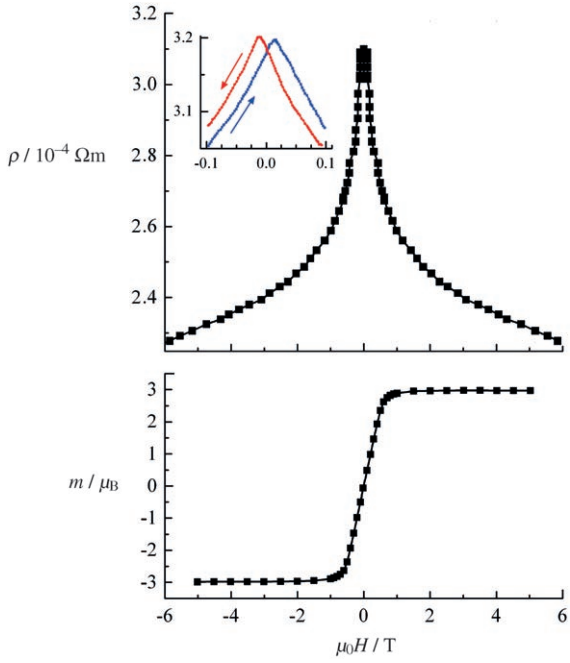

Figure 32. Field dependence of the resistivity (top; inset: enlargement of the low-field region) and the magnetic moment per atom (bottom) of polycrystalline Sr_2FeMoO_6.[35]

Chromium doping of the parent compound Sr_2FeReO_6 leads to non-monotonic behavior for the saturation magnetization and to an enhancement of the magnetic moment for doping levels up to 10%. The Curie temperature increases monotonically from 401 to 616 K. In contrast, zinc doping leads to a continuous decrease in the saturation magnetization and the Curie temperature. At a chromium doping level of 40%, a phase transition from a tetragonal to a cubic structure occurs. For zinc-doped samples, the tetragonal distortion increases linearly with increasing zinc content.

The oxidation state of iron, which has a strong influence on the structure, was determined by ^{57}Fe Mössbauer spectroscopy to be $+2.7$ for Sr_2FeReO_6.[166] As determined by magnetic-susceptibility measurements, the ferrimagnetic behavior of Sr_2FeReO_6 changes to antiferromagnetic upon partial substitution of rhenium by antimony. ^{57}Fe and ^{121}Sb Mössbauer spectroscopy indicate that the valence state of antimony in $Sr_2FeRe_{1-x}Sb_xO_6$ is $+5$ over the entire substitution range ($0 \le x \le 1$), whereas the valence state of iron changes from $+2.7$ for the parent compound to $+2.9$ for $Sr_2FeRe_{0.1}Sb_{0.9}O_6$. In the compounds in which rhenium has been almost completely replaced by antimony, iron takes over rhenium's role as the electronic buffer element. As a consequence, the replacement of the rhenium by a non-magnetic main-group element, such as antimony, blocks the -Fe-O-Re(Sb)-O-Fe- superexchange pathways along the axes of the double-perovskite unit cell, and destroys the itinerant magnetism of the parent compound.[167] Very recently, we have learned of the semiconducting ferromagnetic double perovskite Sr_2CrOsO_6, which has an extraordinary high Curie temperature of 725 K. To date, this compound could only be synthesized under high oxygen pressures.[168]

6.2. Chromium Dioxide

At present, CrO_2 is the only oxide known to exhibit both metallic and ferromagnetic ($T_C = 400$ K) properties. This compound is widely used in magnetic recording devices. On the basis of electronic-structure calculations, CrO_2 was predicted to be half-metallic.[169] CrO_2 crystallizes in the rutile structure (Figure 33), has an integer magnetic moment of $2\mu_B$ per chromium atom, at least at low temperatures, as a saturated ferromagnet (one spin sub-band is completely filled, whereas the other is empty). Spin-resolved photoemission experiments at room temperature and vacuum tunneling experiments at low temperatures reveal nearly complete spin polarization at 2 eV below the Fermi energy, but a negligible DOS at the Fermi level, which is inconsistent with metallic behavior.[34] The half-metallic character of CrO_2 has a straightforward origin: the exchange splitting (the energy difference between the majority and minority bands) is larger than the width of the band occupied by the spin-up electrons; thus, all of the valence electrons of chromium are spin-up, and none are spin-down. CrO_2 is, therefore, fully polarized, as can be seen in Figure 34.

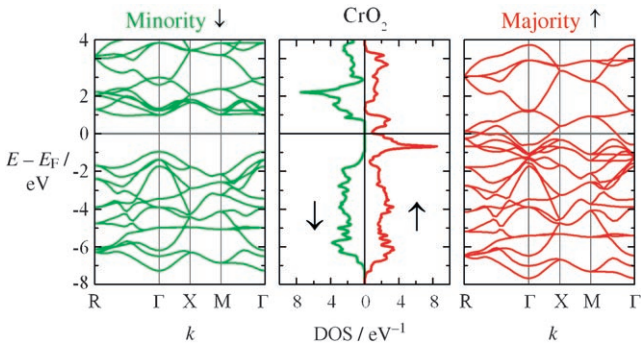

Figure 34. Spin-polarized band structure (left and right) and DOS curve (middle) for CrO_2.

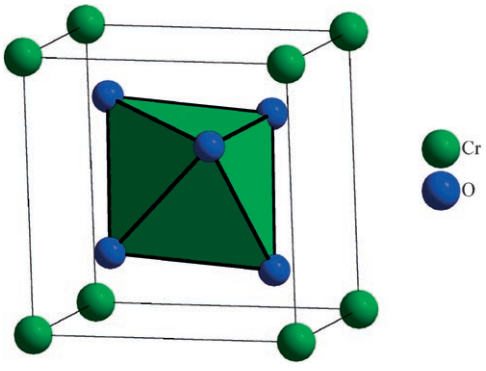

Figure 33. Structure of rutile-type CrO_2.

Because of its full spin polarization, CrO_2 is of paramount interest as a material for spintronic devices.[95] Low-field TMR was observed for films of half-metallic CrO_2 grown by the high-pressure thermal decomposition of CrO_3. Through the surface decomposition of CrO_2 by high-temperature annealing, the intergrain barriers of the films were modified such that insulating Cr_2O_3 formed, leading to a threefold enhancement of the low-field MR. This enhancement indicates the potential of this simple method for the direct control of the interface-barrier characteristics that determine the magnetotransport properties. Studies on a single crystal of CrO_2 revealed a small MR below the transition temperature; for polycrystalline CrO_2, PMR was observed in low fields.[170]

CrO_2 exhibits complex magnetotransport properties.[171,172] The dependence of the Hall resistance on the magnetic field at temperatures of 4 to 100 K differs from that characteristically observed for ferromagnetic metals, and has both hole and electron contributions. According to a two-band model, CrO_2 should have highly mobile holes that move coherently with the more abundant, but less mobile electrons. This hypothesis implies that the band structure of the material may be more complex than that predicted by calculations. However, all spin-polarization-related kinetic characteristics[173] and the results of tunneling spectroscopy experiments[174] indicate that all of the charge carriers in CrO_2 are spin-polarized at low temperatures.

Very recently, Keizer et al. were able to induce a spin-triplet supercurrent through the half-metallic ferromagnet CrO_2.[175] Ferromagnetism should exclude superconductivity, but even iron itself becomes superconducting under pres-

sure.[271] Subsequent to the theoretical predictions of Bergeret et al.,[176] Keizer et al. constructed a Josephson junction by using the strong ferromagnet CrO_2. A conversion from singlet pairs (Cooper pairs) to triplet pairs is predicted to occur at the ferromagnet interface; thus, spin-triplet superconductivity can be induced in a ferromagnet.

CrO_2 is a good candidate for use as a spin source or as a spin detector in spintronic devices. Owing to its high Curie temperature of 400 K, CrO_2 does not exhibit large MR at room temperature.

6.3. Magnetite and Other Spinel Compounds

Magnetite (Fe_3O_4), the most well-known magnetic mineral, is a half-metallic ferrimagnet with a very high Curie temperature (860 K). The iron oxide belongs to the class of spinel compounds, which have the general formula AB_2O_4 (A, B = metals). The spinel $LiTi_2O_4$ was the first oxide superconductor with a transition temperature exceeding 10 K.[177] LiV_2O_4 exhibits all the characteristics of a heavy-Fermion system with an effective mass enhancement on the order of 100, and was the first d-electron system to do so.[178] $LiMn_2O_4$ is a very important positive-electrode material for commercial lithium-ion batteries.[179–182] Unequivocal crystallographic evidence has been reported for the real-space ordering of holes and electrons in this material below the first-order phase-transition temperature.[183] In contrast, such evidence has been difficult to obtain for the perovskite manganites that display CMR, which have recently been under intense investigation.[10,77] In addition, the precise nature of the charge ordering in Fe_3O_4, the first material for which a Verwey transition (see below) was observed, remains unclear.[184]

In Fe_3O_4, the B sites of the spinel structure are populated by an equal mixture of Fe^{3+} and Fe^{2+} ions (Figure 35), leading to two electronic configurations at the B site, $t_{2g}^3e_g^2$ and $t_{2g}^4e_g^2$. The A sites contain oppositely magnetized Fe^{3+} ions with a configuration of $t_{2g}^3e_g^2$. The additional electrons associated with the Fe^{2+} ions at the B sites form small polarons (quasiparticles comprising a charge and a local distortion) that hop among the B sites. The resistivity of Fe_3O_4 at 120 K, slightly above the Verwey transition temperature at which the charges order over the B sites, is $10^{-4}\,\Omega$m. High-quality films and crystals have a spin-only moment of $4.0\,\mu_B$ per formula unit at this temperature, reflecting the ferrimagnetic arrangement of the ions at the A and B sites.

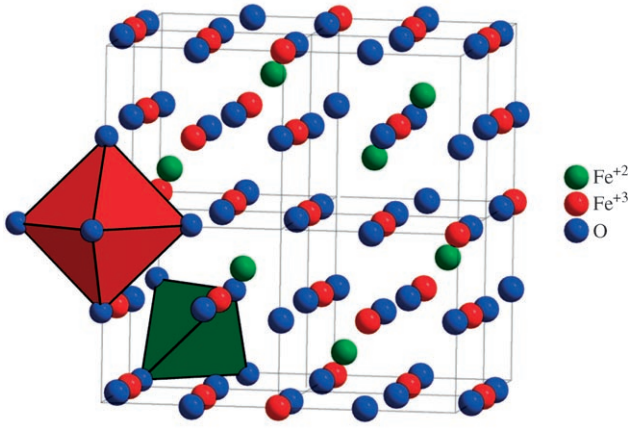

Figure 35. Structure of spinel-type Fe_3O_4 (magnetite).

Magnetite has a spin gap in the majority DOS[161] and is a type-II_B half-metal. Coey et al. compared the MR behavior of Fe_3O_4 as polycrystalline thin films, powder compacts, and single crystals.[34] Negative MR with a maximum value at the coercive field was observed for the thin films and powder compacts, but not for the single crystals. These observations are the result of PMR, the field-induced alignment of the magnetization of the grains. The effect is associated with the intergranular transport of spin-polarized electrons.

MR values of 43% at 4.2 K, and 13% at room temperature were observed in cobalt–alumina–iron oxide tunnel junctions. This large MR is attributed to the presence of a phase with a composition of $Fe_{3-x}O_4$, close to that of half-metallic magnetite, which was identified by electron diffraction. Dedkov et al. investigated the spin-dependent electronic structure of thin epitaxial films of Fe_3O_4(111) at room temperature by means of spin-, energy-, and angle-resolved photoemission spectroscopy.[185] Near the Fermi energy, a spin polarization of 80 ± 5% was found. The electronic structure of Fe_3O_4 (Figure 36) is similar to that of superconducting $LiTi_2O_4$.

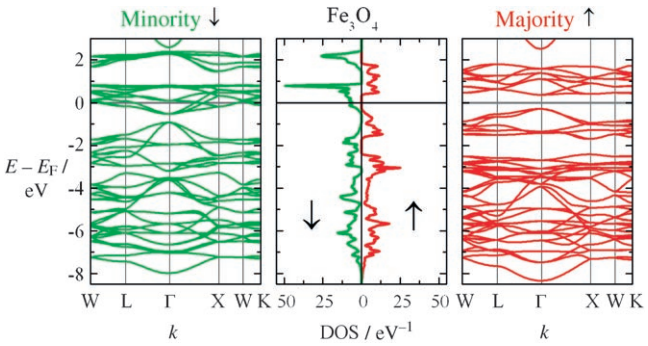

Figure 36. Spin-polarized band structure (left and right) and DOS curve (middle) for Fe_3O_4.

Basu et al. studied the magnetization and MR of the geometrically frustrated spinel $LiMn_2O_4$ near its charge-ordering temperature of 280 K.[186] In a magnetic field of 7 T, a large negative MR of approximately 20% was observed near this temperature. The MR exhibited significant field hysteresis, which was not reflected by the magnetization. This behavior is substantially different from that associated with the CMR of the perovskite manganites. In the case of $LiMn_2O_4$, the MR arises through a slight lowering of the temperature at which charge ordering takes place when a strong magnetic field is applied. The robust nature of the charge ordering, the semiconducting behavior both above and below the transition, and the decoupling of charge and spin degrees of freedom (distinct charge- and magnetic-ordering transitions) all suggest a similarity between $LiMn_2O_4$ and the perovskite manganese oxides with more distorted structures and, therefore, narrow conduction bands.

The electronic structures of $LiTi_2O_4$, $LiMn_2O_4$, and Fe_3O_4, three different spinels, all contain Van Hove singularities near the Fermi level. The compounds are "isovalent", if local magnetic moments are ignored. The $Ti^{3.5+}$ ions in $LiTi_2O_4$ have a $t_{2g}^{0.5}$ configuration. The $Fe^{2.5+}$ ions in the octahedral B sites of Fe_3O_4 have a $t_{2g}^{0.5}$ configuration with respect to the minority 3d states, but a $t_{2g}^{3}e_g^{2}$ configuration with respect to the fully occupied majority 3d states. In $LiMn_2O_4$, the $Mn^{3.5+}$ ions have a $3d^{3.5}$ configuration, with a fully occupied majority t_{2g} band (t_{2g}^{3}), and a $t_{2g}^{0.5}$ configuration with respect to the minority states.

A half-metallic character was proposed for $LiCr_2O_4$, in which the $Cr^{3.5+}$ ions have a $3d^{2.5}$ electronic configuration. However, the electronic structure of $LiCr_2O_4$ is substantially different from that of the closely related half-metal CrO_2, which adopts the rutile structure. A smaller conduction band width was found for $LiCr_2O_4$, perhaps because of the distinct topology of the spinel structure.[187] As the $3d^3$ configuration for a Cr^{3+} ion in an octahedral site is stable, it may be difficult to synthesize a compound containing $Cr^{3.5+}$ ions.

Half-metallicity was first suggested in 1982 by Horikawa et al., after they calculated the electronic structure of the spinel $CuCr_2S_4$.[188] The magnetic configuration of $CuCr_2S_4$ can be described in terms of two Cr^{3+} ions (each with a spin-up $3d^3$ configuration) and one Cu^{2+} ion (with a spin-down $3d^9$ configuration). Each Cr^{3+} ion has a moment of $3\mu_B$, and the Cu^{2+} ion has a moment of $1\mu_B$ in the opposite direction. As a result, $CuCr_2S_4$ has a net moment of $5\mu_B$ per formula unit. In combination with metallic conductivity, an integer value of the spin-only moment is a central feature of half-metallic character.

6.4. Cubic and Hexagonal XYZ Compounds

NiMnSb, which crystallizes in the cubic $C1_b$ structure (XYZ), was one of the first materials for which half-metallic ferromagnetism was predicted.[3] This compound is especially well-suited for applications because of its high Curie temperature of 730 K. Later experiments, for example positron annihilation, confirmed that bulk NiMnSb is a half-metallic ferromagnet.[189,190] However, surface-sensitive techniques, such as photoemission spectroscopy, detected a highly reduced spin polarization.[191,192] In contrast to theoretical expectations, Andreev-reflection measurements on a thin film of NiMnSb grown by three-source co-evaporation revealed a polarization of only 58%.[95] Tunneling experiments on NiMnSb–Al_2O_3–Al junctions revealed a polarization of only 28% in epitaxial NiMnSb.[193] Therefore, a complete control over the interfaces and surfaces of these materials is of crucial importance. Suga et al. reported a local magnetic moment of $3.62\mu_B$ at the manganese site of NiMnSb, and small magnetic moments at the nickel and antimony sites, in agreement with theoretical predictions.[194]

On the basis of the electronegativities of the component elements, NiMnSb would be better described as MnNiSb. In addition to the Slater–Pauling rule, another rule must taken into account for the manganese atoms at the Y position of the $C1_b$ structure. Kübler found that the manganese atoms exhibit a high, localized magnetic moment.[56,196] According to electronic-structure calculations, the manganese atoms have a magnetic moment of approximately $4\mu_B$. The manganese atoms may be formally described as Mn^{3+} ions with a $3d^4$ ($t_{2g}^{3}e_g^{1}$) configuration. Other manganese-containing $C1_b$ compounds with the preferred 22-electron configuration are PdMnSb, PtMnSb, and AuMnSn.

Bojin and Hoffmann reported on the structure–property relationships of the REME phases (RE = rare earth or early transition metal, M = late transition metal, E = main-group element).[197] There are more than 2000 compounds with this composition. These phases are interesting because of their unusual electronic and magnetic properties.

The most common electron counts are 18 or 19 valence electrons per formula unit for REME compounds containing anionic $[ME]^{n-}$ substructures with wurtzite-type or zinc-blende-type arrangements. In contrast to the zinc-blende structure, the wurtzite structure has a free *c*/*a* ratio and a free *z* parameter for one atom, which determines the puckering of the lattice: the two extremes are the graphite sheets of the AlB_2 structure, or the wurtzite lattice. The f electrons of the rare earths are localized and are, therefore, not considered as valence electrons. Depending on the ionic radius of the rare-earth ion, the REME compound crystallizes in either a cubic structure, or a hexagonal structure containing a more or less puckered anionic sublattice.

Approximately 50 hexagonal compounds crystallize in the LiGaGe structure, which can be thought of as a RE^{n+} ion stuffed into a wurtzite $[ME]^{n-}$ sublattice.[63] Note that many compounds originally assigned to the $CaIn_2$ structure (with the M and E atoms randomly distributed over the wurtzite sublattice) actually adopt the LiGaGe structure (with the M and E atoms ordered over the wurtzite lattice).[198–200] It was recently shown that 18-valence-electron compounds with the LiGaGe structure are closed-shell species, which are non-magnetic and semiconducting, or at least have a pseudogap at the Fermi energy.[63] The electronic structure is also strongly dependent on the *z* parameter of the crystal structure. If the sheets are planar (graphite-type), then the bonding interactions are exclusively within the sheets. In the case of 18 valence electrons, the electronic structure is two-dimensional and has only a pseudogap at the Fermi energy. Increasing the interactions between the layers in the third dimension through puckering leads to a gap at the Fermi level and semiconducting behavior.

As discussed above, hexagonal GdAuSn can be described as Gd^{3+} ions stuffed into a $[AuSn]^{3-}$ sublattice. Several studies have been carried out on this compound;[200–202] however, the interpretations were only supported by powder X-ray diffraction, which could not provide the precise structural parameters necessary for a band-structure analysis. Future work must, therefore, concentrate on the preparation and characterization of single crystals.

6.5. Heusler Compounds

The potential of Heusler compounds (X_2YZ) as half-metallic ferromagnets has been known for more than 20 years.

Kübler et al. were the first to recognize that the minority DOS at the Fermi energy nearly vanishes for Co_2MnAl and Co_2MnSn.[62] They concluded that this electronic situation should lead to peculiar transport properties for these Heusler compounds, because only the majority electrons contribute to conduction. Most of these compounds should have complete spin polarization at the Fermi energy.[57,69,203,204]

However, because of the first disappointing results for Heusler compounds in multilayer GMR systems, the number of groups working in this area was originally small. With the discovery of large negative MR for $Co_2Cr_{0.6}Fe_{0.4}Al$ and the general success of tunnel junctions, a renaissance began in the study Heusler compounds. Band-structure calculations predicted that the "ordered" ($L2_1$) Heusler compounds Co_2CrAl and $Co_2Cr_{0.6}Fe_{0.4}Al$ should exhibit a complete spin polarization at the Fermi energy.[37] For $Co_2Cr_{0.6}Fe_{0.4}Al$, the DOS curve, which exhibits a Van Hove singularity in the vicinity of the Fermi energy in the majority spin channel, and a gap in the minority spin channel, indicates half-metallic ferromagnetism. This unique band structure makes $Co_2Cr_{0.6}Fe_{0.4}Al$ a potential candidate for large MR. In a low magnetic field of 0.1 T at room temperature, a MR of 30% was indeed found for pressed-powder pellets.[37] This observation was the motivation for considerable effort to understand and exploit the unusual electronic properties of $Co_2Cr_{1-x}Fe_xAl$.

Recent band-structure calculations confirmed the half-metallic character of the chromium-rich compounds.[69,205–208] Zhang et al. found that Co_2CrAl is a true half-metallic ferromagnet with a magnetic moment of $3\,\mu_B$, in agreement with the Slater–Pauling rule.[208] Using "superstructure calculations", Kobayashi et al. investigated $Co_2Cr_{1-x}Fe_xAl$ for varying values of x.[209] For $x \geq 0.625$, the half-metallicity is destroyed. The replacement of chromium by iron may be considered as electron doping, which disrupts the electronic properties by shifting the energy of the Van Hove singularity relative to the Fermi level. However, such a rigid-band model is often too simple to allow an accurate prediction of the effects of doping.[69,207]

Band-structure calculations for disordered variants of $Co_2Cr_{1-x}Fe_xAl$ also confirm a strongly reduced magnetic moment, as well as a loss of the half-metallic character. Using the coherent-potential approximation (CPA), Miura et al. investigated the effects of disorder on the electronic and magnetic properties of $Co_2Cr_{1-x}Fe_xAl$.[206] They found that the complete spin polarization is only retained up to approximately 10% B2-like disorder (a mixing of atoms over the Y and Z sites).[206,207] However, the spin polarization remains high for even the completely B2-disordered alloy. A small amount of disorder between the cobalt atoms at the X sites and the chromium or iron atoms at the Y sites causes a larger decrease in the spin polarization.

Using point-contact spectroscopy, Clifford et al. found a spin polarization of up to 80% for $Co_2Cr_{0.6}Fe_{0.4}Al$.[210] In addition to the bulk properties, Galanakis also investigated the influence of surface states on the half-metallic properties of Heusler compounds.[211] He reported that Co_2CrAl with a CrAl-terminated surface behaves differently from all other Heusler compounds, the half-metallic properties being retained at the surface.

For Co_2CrAl, a magnetic moment of approximately $1.56\,\mu_B$ per formula unit was measured by Buschow and van Engen.[195] It was thought that the magnetic moment in this material is mainly carried by the cobalt atoms, the contribution of the chromium and aluminum atoms being small. According to recent band-structure calculations, all of the constituents of Co_2CrAl should possess a magnetic moment: per atom, $0.77\,\mu_B$ for cobalt, $1.63\,\mu_B$ for chromium, and $-0.10\,\mu_B$ for aluminum. The total moment is approximately $3\,\mu_B$ per formula, in agreement with the Slater–Pauling rule for the magnetic moment of half-metallic Heusler compounds containing 3d transition metals [Eq. (10)]. According to several band-structure calculations, the DOS of Co_2CrAl exhibits half-metallic character. In particular, the DOS curve has a gap at the Fermi level in the minority band and a high DOS in the majority band. This property is conserved when chromium is partially replaced by iron. Therefore, iron-doping is promising way to tune the electronic properties, that is, to shift a Van Hove singularity to the Fermi edge. As expected, band-structure calculations reveal that a rigid-band model is too simple to correctly predict the effect of this type of doping.[69,207]

A comparison of the experimental results with the calculations demonstrates that site disorder is the main obstacle in the preparation of half-metallic compounds. The preparation of films of $L2_1$-ordered $Co_2Cr_{1-x}Fe_xAl$ is particularly difficult. While the B2-type disorder that results from a partial exchange of chromium or iron atoms with aluminum atoms affect the spin polarization only slightly or not at all, a partial exchange of cobalt atoms with chromium, iron, or aluminum atoms (A2-type disorder) destroys the half-metallic character immediately. The element-specific measurement of the chromium moment is an efficient tool for characterizing this type of disorder in $Co_2Cr_{1-x}Fe_xAl$.[207,212,213]

The family of Heusler compounds (X_2YZ) is very large, but only a few of the members exhibiting half-metallic ferromagnetism do not contain cobalt in the X site. The first experiments on cobalt-based Heusler compounds were reported by Webster et al.[214,215] Since then, Heusler compounds containing cobalt and manganese have attracted considerable attention because they have high Curie temperatures (above 900 K).[71,72] One of these compounds, Co_2MnSi, is an attractive candidate for many spin-dependent applications. Despite strong evidence in some cases, half-metallic ferromagnetism in Heusler compounds containing cobalt and manganese, especially at high temperatures, has never been unambiguously confirmed by experiment. Co_2FeSi is a good candidate for obtaining such evidence, as it has the highest Curie temperature and the highest magnetic moment yet observed for a Heusler compound.[52,216–218]

The electronic structure plays an important role in determining the magnetic properties of Heusler compounds, in particular, the occurrence of half-metallic ferromagnetism. Band-structure calculations must, therefore, be performed very carefully, and all of the approximations made must be considered when discussing the results.

The first attempts to calculate the band structures of some cobalt-based Heusler compounds ($X = Co$) did not indicate half-metallic ferromagnetism.[219] According to these calcu-

lations, a minimum occurs in the DOS at the Fermi level, but the minority bands cross the Fermi energy. At that time, the calculations were based on spherical potentials, and the exchange-correlation potential of the local spin-density approximation (LSDA) was used in a rather simple form.[220–223] The first clear indication of half-metallic ferromagnetism in cobalt- and ruthenium-based Heusler compounds was reported by Ishida et al. for Co_2MnZ and Ru_2MnZ (Z = Al, Si, Sn, Sb).[224,225] Using full-symmetry potentials, Mohn et al. found a magnetic ground state for Co_2TiZ (Z = Al, Sn), but not a half-metallic state.[226]

Galanakis et al. reported half-metallic behavior for various X_2YZ Heusler compounds, but not for compounds with X = Co and Y = Ti or Fe.[203] These results were compatible with those for Y = Mn compounds calculated by Picozzi et al. using the generalized gradient approximation (GGA) instead of the pure LSDA.[204] The GGA, as introduced by Perdew et al., accounts for density gradients, which are not considered in the pure LSDA parameterization of the exchange-correlation functional.[227–230] Using spherical potentials and the GGA, a half-metallic state was not found for Co_2FeAl.[206,231] However, a half-metallic ferromagnetic ground state was found for the complete series $Co_2Cr_{1-x}Fe_xAl$ in calculations using full-symmetry potentials and the GGA.[69] This result clearly indicates that to find the correct ground states of the Heusler compounds, electronic-structure calculations must include both full-symmetry potentials and the GGA.

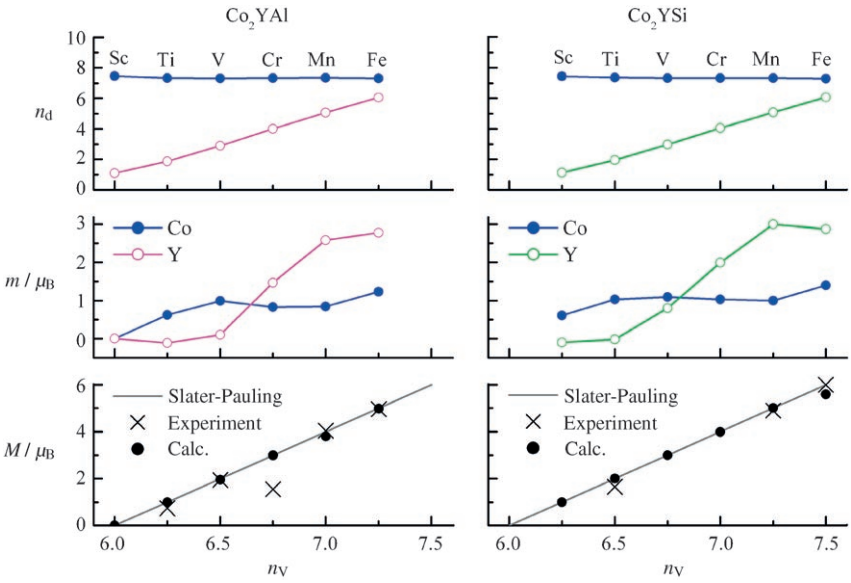

Figure 37. Distribution of the 3d electrons n_d (top) and the magnetic moment per atom (middle) as a function of the mean number of valence electrons per atom in Co_2YAl (left) and Co_2YSi (right; Y = Sc–Fe). Comparison of the experimental and calculated magnetic moments per formula unit to the Slater–Pauling rule (bottom).

The properties of cobalt-based Heusler compounds were calculated using this approach, and it was found that most follow the Slater–Pauling rule. However, the question remains as to how the electrons must be distributed to produce half-metallic ferromagnetism. As the s and p electrons do not contribute to the magnetic moment, it is sufficient to consider the d electrons. The valence d electrons are sufficiently localized to be assigned to the different atoms, whereas most of the valence s and p electrons are completely delocalized. The results are summarized in Figure 37. For the complete series Co_2YZ (Y = Sc–Fe, Z = Al, Si), it is found that approximately 7.3 d electrons are located at the cobalt site; that is, cobalt has an approximate $3d^{7.5}$ configuration in all of the compounds. The number of 3d electrons at the Y site increases linearly with the atomic number, resulting in configurations of $3d^1$–$3d^6$ for scandium to iron. The magnetic moment at the cobalt atoms is approximately $1\mu_B$ for Co_2YSi with Y = Ti–Mn, and is slightly lower for Co_2YAl with Y = V–Fe. Regardless of the type of atom at the Z site, scandium and titanium atoms at the Y site do not contribute to the magnetic moment. However, the total moment still follows the Slater–Pauling rule, which means that the cobalt moment must be reduced when the Y site is occupied by the lighter transition metals (in a manner depending on whether Z is Al or Si). For the heavier transition metals, V–Fe, the moment varies from 0 to $4\mu_B$, depending on the element at the Z site. To reach the expected total moment of $6\mu_B$ for Co_2FeSi, a larger moment is necessary for both the cobalt and the iron atoms. However, for this compound in particular, the LSDA-GGA calculations fail to give the expected moment, even when full-symmetry potentials are used. From the behavior of the moment attributed to the cobalt atoms, in particular, its stabilization at approximately $1\mu_B$, it is clear that interactions between the cobalt atoms play an important role in the half-metallic ferromagnetism of the cobalt-based Heusler compounds. Note that such interactions are absent in the $C1_b$ compounds.

To explain the magnetic properties of Co_2FeSi (for example, the total moment of $6\mu_B$),[52] the partial localization of the 3d electrons and the correlation between them must be discussed. The relative importance of the itinerant and localized properties of d electrons in metal alloys has been discussed by Slater,[49,232] van Vleck,[233,234] and Goldmann.[235] As was first mentioned by Pauling for Cu_2MnAl,[50] Heusler compounds are generally thought of as systems with localized magnetic moments. On the other hand, d electrons are normally delocalized in metals. The question of correlation in transition-metal compounds then becomes the following: to what extent are the on-site Coulomb interactions between the d electrons preserved, despite shielding by delocalized electrons, so that important atomic properties such as Hund's rules are obeyed and partially determine the magnetic properties?[236]

To answer this question, band-structure calculations were carried out by using the LDA + U method,[237] one of the most popular and easiest approaches to include on-site electron–electron correlations at the transition metals.[238] The LDA + U method takes into account the orbital dependence of the

Coulomb and exchange interactions, which is not considered in the pure LSDA. In this method, the effective Coulomb exchange interaction $U_{eff} = U - J$, where U is the Coulomb integral and J the exchange integral, is used to include the double-counting correction. The calculations were performed for the series $Co_2Mn_{1-x}Fe_xSi$ ($0 \le x \le 1$). Independent of the iron concentration, the values of U_{eff} were set to $U_{Co} = 1.9$ eV, $U_{Fe} = 1.795$ eV, and $U_{Mn} = 1.768$ eV. In previous work, the use of these semi-empirical values in the LDS + U method was found to accurately describe the experimentally determined magnetic states of Co_2MnSi and Co_2FeSi.[238] These U_{eff} values are similar to those reported by Bandyopadhyay and Sarma for the Coulomb interaction U_{dd} between 3d electrons in the elemental first-row transition metals prior to the introduction of the LDA + U method.[239] A plot of the magnetic moment per formula unit determined from the LDA + U calculations as a function of the iron concentration closely follows the Slater–Pauling curve and is in good agreement with experiment (Figure 38). The Fermi level shifts relative to the

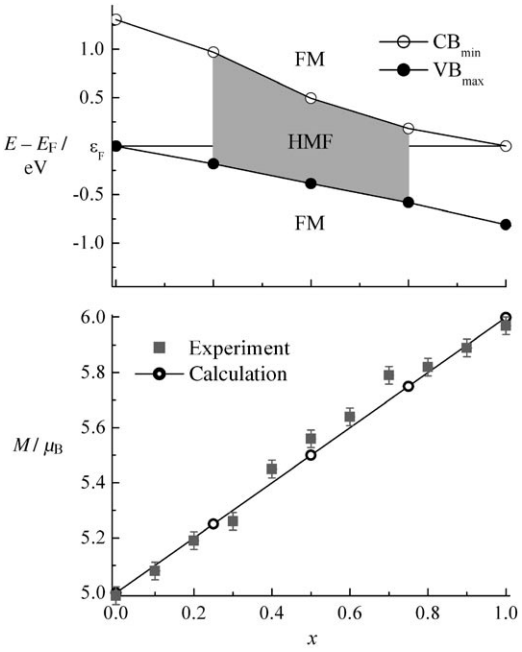

Figure 38. Dependence of the position of the minority band gap of $Co_2Mn_{1-x}Fe_xSi$ on x (top); CB = conduction band, VB = valence band, FM = ferromagnetism, HMF = half-metallic ferromagnetism. Comparison of the experimental and calculated magnetic moments per formula unit to the Slater–Pauling rule (bottom).

minority band gap, from the top of the minority valence band for Co_2MnSi to the bottom of the minority conduction band for Co_2FeSi. In contrast to the results of calculations neglecting on-site correlation, $Co_2Mn_{1-x}Fe_xSi$ remains half-metallic over the entire range of the iron concentrations according to LDA + U calculations with a single set of Coulomb exchange parameters. These findings strongly support the assumption that electron–electron correlation should not be neglected in Heusler compounds.

The electronic structure of the series $Co_2Mn_{1-x}Fe_xSi$ was very recently investigated by means of high-resolution HXPS.[240,241] The high photon energy of 8 keV used ensured a true bulk sensitivity, owing to the large escape depth of 115 Å. In Figure 39, the valence-band HXPS spectra are compared to the calculated total DOS curves. The spectra

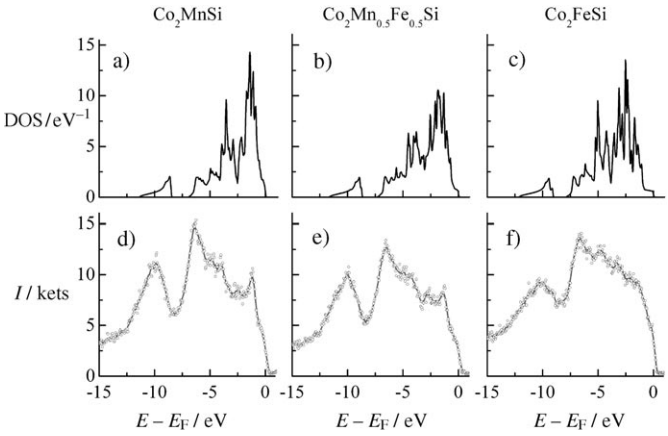

Figure 39. Comparison of the weighted DOS curves for a) Co_2MnSi, b) $Co_2Mn_{0.5}Fe_{0.5}Si$, and c) Co_2FeSi to their valence-band HXPS spectra in (d), (e), and (f), respectively.

agree well with the calculated DOS curves and, thus, justify the use of the LDA + U method. In particular, the shape of the spectra near the Fermi energy can only be explained through the assumption of band gaps in the minority states and, thus, provides indirect evidence for half-metallic states in all three compounds. As further evidence for a band gap, however, spin-resolved photoemission spectra at high energies would be highly desirable.

6.6. Magnetoresistance in Half-Metallic Intermetallics

From TMR data for a system with one electrode consisting of a Co_2MnSi film, Schmalhorst et al. inferred a spin polarization of 61 % at the barrier interface.[242,243] Although the desired spin polarization of 100 % was not reached, the experimental value of the spin polarization is larger than the maximum value of 55 % measured for a variety of 3d-transition-metal alloys in combination with Al_2O_3 barriers.[244] Tunneling junctions with $Co_2Cr_{0.6}Fe_{0.4}Al$ electrodes were fabricated by several groups.[245–247] Spin-valve-type tunneling junctions consisting of $Co_2Cr_{0.6}Fe_{0.4}Al$–AlO_x(1.4 nm)–CoFe layers were prepared at room temperature by sputtering onto a thermally oxidized silicon substrate without any buffer layers.[246] In this case, the $Co_2Cr_{1-x}Fe_xAl$ films were polycrystalline with a B2-like structure. The maximum TMR was obtained for $x = 0.4$, with values of 19 % at room temperature and 27 % at 5 K.[246] The TMR of 27 % corresponds to a spin polarization of 30 % for $Co_2Cr_{0.6}Fe_{0.4}Al$, if a spin polarization of 50 % is assumed for the CoFe alloy in the Jullière equation.

Tunnel junctions consisting of $Co_2Cr_{0.6}Fe_{0.4}Al$–AlO_x-(1.4 nm)–Co were also prepared on Al_2O_3(110).[248] In this case, the films were sputtered at 600 K, far below the optimum growth temperature of 1000 K, and had smooth

surfaces, but were polycrystalline.[247] The maximum TMR values were 10.8% at 4 K and 6% at room temperature,[248] somewhat smaller than those reported earlier for similar electrodes.[246] The smaller TMR values may be a result of the fact that the cobalt electrode was not optimized to prevent a switching of both electrodes at the critical field.[248] The observed magnetization loops indicate that the two electrodes were not aligned completely antiparallel to one another at zero field, leading to a reduced TMR.

Recently, Marukame et al. achieved a TMR of 240% at 4.2 K for a $Co_2Cr_{0.6}Fe_{0.4}Al$–MgO–CoFe tunnel junction.[249] This value corresponds to a spin polarization of 79% at low temperatures (50% at room temperature), in agreement with calculations for the disordered B2 alloy $Co_2Cr_{0.6}Fe_{0.4}Al$. The largest TMR at room temperature was found very recently by Inomata and co-workers for a system incorporating the quaternary Heusler compound $Co_2FeAl_{0.5}Si_{0.5}$.[250] $L2_1$-ordered samples exhibited a TMR of 180% at 300 K. Magnetic tunnel junctions with the stacking structure Co_2MnSi–AlO_x–Co_2MnSi exhibited an extremely large TMR of 570% at low temperatures, which is the largest TMR effect yet reported for a system with an amorphous AlO_x tunneling barrier.[251] The bias-voltage dependence of the tunneling conductance for Co_2MnSi indicated a half-metallic gap of 350–400 meV, with an energy separation of just 10 meV between the Fermi energy and the bottom edge of the conduction band.[252] This small energy separation could explain the unfavorable temperature dependence of the TMR. The evolution of TMR over the last eight years is illustrated in Figure 40.

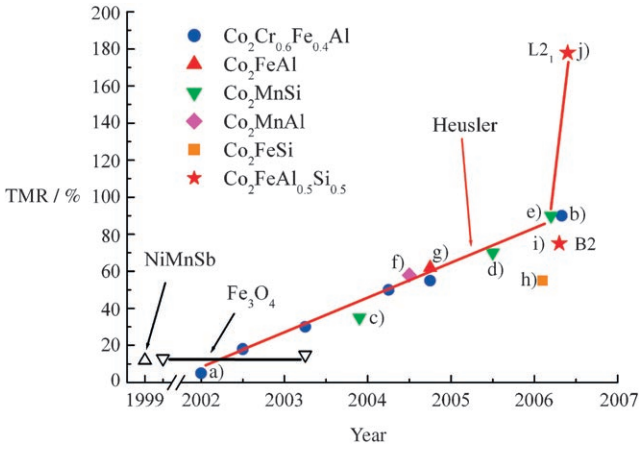

Figure 40. Evolution of TMR for half-metallic ferromagnets at room temperature since 1999. a) Ref. [245]; b) Ref. [263]; c) Ref. [264]; d) Ref. [265]; e) Ref. [251]; f) Ref. [266]; g) Ref. [267]; h) Ref. [268]; i) Ref. [269]; j) Ref. [250].

There are a few covalent half-metals that exhibit CMR. Many of the $C1_b$ compounds and some of the Heusler compounds are semiconductors[58,59,253,254] and undergo a semiconductor–metal transition when doped with electrons or holes. A few of these compounds become half-metallic ferromagnets and exhibit MR of comparable magnitude to that of the perovskite manganites. Large MR has been observed for $Fe_{2+x}V_{1-x}Al$,[255] $Fe_{2+x}V_{1-x}Ga$,[255] $Fe_{3-x}V_xSi$,[256] Co_2TiSn,[257] $CoV_{0.6}Mn_{0.4}Sb$,[258] and RENiSb (RE = Tb, Dy, Ho).[258,270] For example, a CMR of approximately 40% was found for $Fe_{2.1}V_{0.9}Al$ at 4 K.[253] RENiSb are semiconductors or semimetals.[258,259]

The solid solutions $NiTi_{1-x}Mn_xSb$ and $CoV_{1-x}Mn_xSb$ were reported to exhibit CMR by Pierre et al.[260] As shown by magnetic measurements and electronic-structure calculations, the manganese 3d states in these compounds are localized for low manganese concentrations. In $CoV_{1-x}Mn_xSb$, the magnetic interactions suddenly and strongly increase near $x \approx 0.4$, and semiconducting behavior is observed in the range $0.35 \leq x \leq 0.45$. These features were tentatively explained on the basis of an Anderson localization of 3d states in these disordered alloys. Large MR is observed near the magnetic ordering temperature for some phases.[258] The CMR exhibited by $CoV_{0.6}Mn_{0.4}Sb$ is surprising because CoVSb and CoMnSb are both metals. However, a careful study of the band structure of $CoV_{0.6}Mn_{0.4}Sb$ indicates that a Van Hove singularity occurs near the Fermi level, which could be a possible explanation for this exceptional behavior.

7. Conclusions: Is There a Simple Recipe?

Achieving specific properties in inorganic compounds by materials design remains a challenge, and a revolutionary breakthrough often appears to be distant. A more realistic goal is to screen existing materials in a rational manner for interesting properties, such as half-metallic ferromagnetism, superconductivity, or CMR. Another possibility is to carefully examine the crystal and electronic structures of materials that are candidates for possessing the desired properties.

A few attempts were made to develop recipes for half-metallic ferromagnets[3,34,92] and for compounds exhibiting CMR.[36,261] All of these ideas were based on the analysis of the electronic structures of several compounds and a chemical or physical interpretation, depending on the background of the scientist. Using density functional theory (DFT) calculations, Felser et al. systematically investigated the electronic structures of many materials exhibiting CMR.[36] In addition to the dominant ferromagnetic coupling, certain features stand out in the spin-polarized electronic structures of these compounds. Two bands play a pivotal role in the electronic structures: one localized magnetic band located just below the Fermi energy, and another (possibly broader) conduction band that is polarized by the first. Elemental gadolinium, which exhibits the largest negative MR of the elements, also has such a two-band electronic structure. In contrast, ferromagnetic metals, such as iron (which exhibits a very small MR), do not have well-separated localized magnetic and extended conduction bands. How the spin differentiation is induced is not clear, but structural features such as low dimensionality might play a role. Such structural features could possibly be manifested as instabilities in the electronic structure, for example, Van Hove singularities in the vicinity of the Fermi energy. The two-band model for CMR is related to the two band-model of Simon for superconductivity.[261]

8. Summary

In this Review, ideas about the design of materials for spintronics were presented. The combination of synthesis and electronic-structure calculations is a powerful tool to identify suitable materials. CMR was discussed on the basis of several classes of materials: perovskite manganites, Ruddlesden–Popper compounds, pyrochlores, spinels, rare-earth compounds, and Zintl compounds. The similarity of the electronic structures of materials exhibiting CMR or superconductivity helped to identify some of these compounds. The role of ferromagnetic semiconductors was pointed out for various examples, from oxides to doped semiconductors. Furthermore, the preconditions for half-metallic ferromagnetism, as a very important property for spintronics, were extensively discussed. Particular attention was given to chemical aspects, such as the importance of covalent and ionic interactions in oxides, $C1_b$ compounds, and Heusler compounds.

In summary, the design of new materials for spintronics remains a challenge for solid-state chemistry.

All calculations presented herein were performed using Wien2K.[262] The authors thank H. A. Dürr (Berlin), M. Greenblatt (Rutgers, USA), Y. Hwu (Taipei, Taiwan), K. Kobayashi (Hyogo, Japan), H.-J. Lin (Hsinchu, Taiwan), J. Morais (Porto Alegre, Brazil), R. Seshadri (Santa Barbara, USA), A. Simon (Stuttgart), as well as F. Casper, A. Jung, V. Jung, H. C. Kandpal, K. Kroth, V. Ksenofontov, G. Schönhense, H. Spiering, U. Stumm, W. Tremel, and S. Wurmehl (Mainz) for their help with theory and experiments, and for fruitful discussions. Assistance by the staff of the synchrotron facilities BESSY (Berlin), LNLS (Campinas, Brazil), NSRRC (Hsinchu, Taiwan), and SPRING-8 (Hyogo, Japan) is gratefully acknowledged. This work was financially supported by the DFG as part of the FG 559, projects TP1 and TP7, as well as by the DAAD through the program PROBRAL (no.: 167-04).

Received: May 9, 2006

[1] I. Zutic, J. Fabian, S. D. Sarma, *Rev. Mod. Phys.* **2004**, *76*, 323.
[2] P. Sharma, *Science* **2005**, *307*, 513.
[3] R. A. de Groot, F. M. Müller, P. G. van Engen, K. H. J. Buschow, *Phys. Rev. Lett.* **1983**, *50*, 2024.
[4] W. Thomson, *Proc. R. Soc. London Ser. A* **1857**, *8*, 546.
[5] G. Binasch, P. Grünberg, F. Saurenbach, W. Zinn, *Phys. Rev. B* **1989**, *39*, 4828.
[6] M. N. Baibich, J. M. Broto, A. Fert, F. N. V. Dau, F. Petroff, *Phys. Rev. Lett.* **1988**, *61*, 2472–2475.
[7] P. Ball, *Nature* **2000**, *404*, 918.
[8] R. von Helmolt, J. Wecker, B. Holzapfel, L. Schultz, K. Samwer, *Phys. Rev. Lett.* **1993**, *71*, 2331.
[9] S. Jin, T. H. Tiefel, M. McCormack, R. A. Fastnacht, R. Ramesh, L. H. Chen, *Science* **1994**, *264*, 413.
[10] C. N. R. Rao, A. K. Cheetham, R. Mahesh, *Chem. Mater.* **1996**, *8*, 2421.
[11] X. J. Chen, H.-U. Habermeier, C. C. Almasan, *Phys. Rev. B* **2003**, *68*, 132407.
[12] P. D. Battle, S. J. Blundell, D. E. Cox, M. A. Green, J. E. Millburn, P. G. Radaelli, M. J. Rosseinsky, L. E. Spring, J. Singleton, J. F. Vente, *Mater. Res. Soc. Symp. Proc.* **1997**, *453*, 331.
[13] G. Briceño, H. Chang, X. Sun, P. G. Schultz, X.-D. Xiang, *Science* **1995**, *270*, 273.
[14] A. P. Ramirez, M. A. Subramanian, *Science* **1997**, *277*, 546.
[15] A. P. Ramirez, R. J. Cava, J. Krajewski, *Nature* **1997**, *386*, 156.
[16] J. Y. Chan, S. M. Kauzlarich, P. Klavins, J. Z. Liu, R. N. Shelton, D. J. Webb, *Phys. Rev. B* **2000**, *61*, 459.
[17] G. A. Petrakovskii, L. I. Ryabinkina, N. I. Kiselev, D. A. Velikanov, A. F. Bovina, G. M. Abramova, *JETP Lett.* **1999**, *69*, 949.
[18] C. Felser, K. Ahn, R. K. Kremer, R. Seshadri, A. Simon, *J. Solid State Chem.* **1999**, *147*, 19.
[19] M. R. Oliver, J. O. Dimmock, A. L. McWhorter, T. B. Reed, *Phys. Rev. B* **1972**, *5*, 1078–1098.
[20] S. von Molnar, A. Briggs, J. Flouquet, G. Remenyi, *Phys. Rev. Lett.* **1983**, *51*, 706.
[21] K. McEwen, G. D. Webber, L. W. Roeland, *Physica B* **1977**, *86–88*, 531.
[22] H. Kim, M. M. Olmstead, P. Klavins, D. J. Webb, S. M. Kauzlarich, *Chem. Mater.* **2002**, *14*, 3382.
[23] D. Sánchez-Portal, R. M. Martin, S. M. Kauzlarich, W. E. Pickett, *Phys. Rev. B* **2002**, *65*, 144414.
[24] J. S. Moodera, J. Nassar, G. Mathon, *Annu. Rev. Mater. Sci.* **1999**, *29*, 381.
[25] P. M. Tedrow, R. Meservey, *Phys. Rev. B* **1973**, *7*, 318.
[26] M. Jullière, *Phys. Lett. A* **1975**, *54*, 225.
[27] S. Maekawa, U. Gäfvert, *IEEE Trans. Magn.* **1982**, *18*, 707.
[28] J. S. Moodera, L. R. Kinder, T. M. Wong, R. Meservey, *Phys. Rev. Lett.* **1995**, *74*, 3272.
[29] T. Miyazaki, N. Tezuka, *J. Magn. Magn. Mater.* **1995**, *139*, L231.
[30] M. Bowen, M. Bibes, A. Barthelemy, J.-P. Contour, A. Anane, Y. Lemaitre, A. Fert, *Appl. Phys. Lett.* **2003**, *82*, 233.
[31] S. S. P. Parkin, C. Kaiser, A. Panchula, P. M. Rice, B. Hughes, M. Samant, S.-H. Yang, *Nat. Mater.* **2004**, *3*, 862.
[32] S. Yuasa, A. Fukushima, T. Nagahama, K. Ando, Y. Suzuki, *Jpn. J. Appl. Phys.* **2004**, *43*, L588.
[33] S. Yuasa, T. Nagahama, A. Fukushima, Y. Suzuki, K. Ando, *Nat. Mater.* **2004**, *3*, 868.
[34] J. M. D. Coey, M. Venkatesan, M. A. Bari in *Lecture Notes in Physics*, *Vol. 595* (Eds.: C. Berthier, L. P. Levy, G. Martinez), Springer, Heidelberg, **2002**, p. 377.
[35] K.-I. Kobayashi, T. Kimura, H. Sawada, K. Terakura, Y. Tokura, *Nature* **1998**, *395*, 677.
[36] C. Felser, R. Seshadri, *Int. J. Inorg. Mater.* **2000**, *2*, 677.
[37] T. Block, C. Felser, G. Jakob, J. Ensling, B. Mühling, P. Gütlich, V. Beaumont, F. Studer, R. J. Cava, *J. Solid State Chem.* **2003**, *176*, 646.
[38] T. Block, S. Wurmehl, J. Windeln, C. Felser, *Appl. Phys. Lett.* **2006**, *88*, 202504.
[39] A. E. Berkowitz, J. R. Mitchell, M. J. Carey, A. P. Young, S. Zhang, F. E. Spada, F. T. Parker, A. Hutten, G. Thomas, *Phys. Rev. Lett.* **1992**, *68*, 3745.
[40] V. A. Ivanov, T. G. Ivanov, V. M. A. Novotortsev, V. T. Kalinnikov, *Russ. Chem. Bull. Int. Ed.* **2004**, *53*, 2357.
[41] H. Munekata, H. Ohno, S. von Molnar, A. Segmüller, L. L. Chang, L. Esaki, *Phys. Rev. Lett.* **1989**, *63*, 1849.
[42] J. M. Kikkawa, I. P. Smorchkova, N. Samarth, D. D. Awschalom, *Science* **1997**, *277*, 1284.
[43] B. T. Jonker, S. C. Erwin, A. Petrou, A. G. Petukhov, *MRS Bull.* **2003**, 740.
[44] H. Ohno, D. Chiba, F. Matsukura, T. Omiya, E. Abe, T. Dietl, Y. Ohno, K. Ohtani, *Nature* **2000**, *408*, 944.
[45] H. Ohno, *Science* **1998**, *281*, 951.
[46] J. A. Gupta, R. Knobel, N. Samarth, D. D. Awschalom, *Science* **2001**, *292*, 2458.

[47] I. Malajovich, J. J. Berry, N. Samarth, D. D. Awschalom, *Nature* **2001**, *411*, 770.
[48] J. Kübler, *Theory of Itinerant Electron Magnetism*, Oxford University Press, New York, **2000**.
[49] J. C. Slater, *Phys. Rev.* **1936**, *49*, 537.
[50] L. Pauling, *Phys. Rev.* **1938**, *54*, 899.
[51] A. P. Malozemoff, A. R. Williams, V. L. Moruzzi, *Phys. Rev. B* **1984**, *29*, 1620.
[52] S. Wurmehl, G. H. Fecher, H. C. Kandpal, V. Ksenofontov, C. Felser, H.-J. Lin, J. Morais, *Phys. Rev. B* **2005**, *72*, 184434.
[53] M. Ležaić, Ph. Mavropoulos, J. Enkovaara, G. Bihlmayer, S. Blügel, *Phys. Rev. Lett.* **2006**, *97*, 026404.
[54] R. Skomski, P. A. Dowben, *Europhys. Lett.* **2002**, *58*, 544.
[55] K. Ghosh, C. J. Lobb, R. L. Greene, S. G. Karabashev, D. A. Shulyatev, A. A. Arsenov, Y. Mukovskii, *Phys. Rev. Lett.* **1998**, *81*, 4740.
[56] J. Kübler, *Physica B* **1984**, *127*, 257.
[57] D. Jung, H. J. Koo, M. H. Whangbo, *J. Mol. Struct. Theochem.* **2000**, *527*, 113.
[58] J. Pierre, R. V. Skolozdra, Y. K. Gorelenko, M. A. Kouacou, *J. Magn. Magn. Mater.* **1994**, *134*, 95.
[59] J. Tobola, J. Pierre, S. Kaprzyk, R. V. Skolozdra, M. A. Kouacou, *J. Phys. Condens. Matter* **1998**, *10*, 1013.
[60] I. Galanakis, *Phys. Rev. B* **2002**, *66*, 012406.
[61] P. Villars, L. D. Calvert, *Pearson's Handbook of Crystallographic Data for Intermetallic Phases*, 2nd ed., ASM International, Materials Park, OH, **1996**.
[62] J. Kübler, A. R. Williams, C. B. Sommers, *Phys. Rev. B* **1983**, *28*, 1745.
[63] H. C. Kandpal, C. Felser, R. Seshadri, *J. Phys. D* **2006**, *39*, 776.
[64] F. Heusler, *Verh. Dtsch. Phys. Ges.* **1903**, *12*, 219.
[65] F. Heusler, W. Starck, E. Haupt, *Verh. Dtsch. Phys. Ges.* **1903**, *5*, 220.
[66] A. J. Bradley, J. W. Rodgers, *Proc. R. Soc. London Ser. A* **1934**, *144*, 340.
[67] G. H. Fecher, S. Wurmehl, H. C. Kandpal, G. Schönhense, C. Felser, *J. Appl. Phys.* **2005**, *99*, 08J106.
[68] I. Galanakis, *J. Phys. Condens. Matter* **2002**, *14*, 6329.
[69] G. H. Fecher, H. C. Kandpal, S. Wurmehl, J. Morais, H.-J. Lin, H.-J. Elmers, G. Schönhense, C. Felser, *J. Phys. Condens. Matter* **2005**, *17*, 7237.
[70] S. Wurmehl, G. H. Fecher, H. C. Kandpal, V. Ksenofontov, C. Felser, *Appl. Phys. Lett.* **2006**, *86*, 032502.
[71] P. J. Webster, K. R. A. Ziebeck in *Alloys and Compounds of d-Elements with Main Group Elements*, *Part 2*, *Vol. 19C* (Ed.: H. P. J. Wijn), Springer, Heidelberg, **1988**, p. 104.
[72] K. R. A. Ziebeck, K.-U. Neumann in *Alloys and Compounds of d-Elements with Main Group Elements*, *Part 2*, *Vol. 32C* (Ed.: H. P. J. Wijn), Springer, Heidelberg, **2001**, p. 64.
[73] H. S. Jarrett, W. H. Cloud, R. J. Bouchard, S. R. Butler, C. G. Frederick, J. L. Gillson, *Phys. Rev. Lett.* **1968**, *21*, 617.
[74] G. L. Zhao, J. Callaway, M. Hayashibara, *Phys. Rev. B* **1993**, *43*, 15781.
[75] I. I. Mazin, *Appl. Phys. Lett.* **2000**, *77*, 3000.
[76] K. Ramesha, R. Seshadri, C. Ederer, T. He, M. A. Subramanian, *Phys. Rev. B* **2004**, *70*, 214409.
[77] J. M. D. Coey, M. Viret, S. von Molnar, *Adv. Phys.* **1999**, *48*, 167.
[78] S. V. Popov, T. Kalinin, T. J. Alvarez, M. Emge, M. Greenblatt, D. A. Bonnell, *Phys. Rev. B* **2002**, *65*, 064426.
[79] H. Ohno, H. Munekata, S. von Molnar, L. L. Chang, in *35th Annual Conference on Magnetism and Magnetic Materials*, *Vol. 69*, AIP, San Diego, **1991**, p. 6103.
[80] H. Ohno, H. Munekata, T. Penney, S. von Molnar, L. L. Chang, *Phys. Rev. Lett.* **1992**, *68*, 2664.
[81] H. Munekata, A. Zaslavsky, P. Fumagalli, R. J. Gambino, *Appl. Phys. Lett.* **1993**, *63*, 2929.
[82] D. Chiba, F. Matsukura, H. Ohno, *Physica E* **2004**, *21*, 966.
[83] H. Akinaga, M. Mizuguchi, K. Ono, M. Oshima, *Appl. Phys. Lett.* **2000**, *76*, 357.
[84] G. H. Jonker, J. H. van Santen, *Physica* **1950**, *16*, 337.
[85] C. Zener, *Phys. Rev.* **1951**, *82*, 403.
[86] P. W. Anderson, H. Hasegawa, *Phys. Rev.* **1955**, *100*, 675.
[87] P. G. de Gennes, *Phys. Rev.* **1960**, *118*, 141.
[88] J. B. Goodenough, *Phys. Rev.* **1955**, *100*, 564.
[89] E. O. Wollan, W. C. Koehler, *Phys. Rev.* **1955**, *100*, 545.
[90] C. W. Searle, S.-T. Wang, *Can. J. Phys.* **1970**, *48*, 2023.
[91] B. Nadgorny, I. I. Mazin, M. Osofsky, R. J. Soulen, Jr., P. Broussard, R. M. Stroud, D. J. Singh, V. G. Harris, A. Arsenov, Y. Mukovskii, *Phys. Rev. B* **2001**, *63*, 184433.
[92] W. E. Pickett, D. J. Singh, *Phys. Rev. B* **1996**, *53*, 1146.
[93] W. E. Pickett, D. Singh, *Physics of Manganites*, Plenum, New York, **1998**.
[94] J.-H. Park, E. Vescovo, H.-J. Kim, C. Kwon, R. Ramesh, T. Venkatesan, *Nature* **1998**, *392*, 794.
[95] R. J. Soulen, Jr., J. M. Byers, M. S. Osofsky, B. Nadgorny, T. Ambrose, S. F. Cheng, P. R. Broussard, C. T. Tanaka, J. Nowak, J. S. Moodera, A. Barry, J. M. D. Coey, *Science* **1998**, *282*, 85.
[96] C. N. R. Rao, A. Arulraj, *Curr. Opin. Solid State Mater. Sci.* **1998**, *3*, 23.
[97] S. N. Ruddlesden, P. Popper, *Acta Crystallogr.* **1958**, *11*, 54.
[98] H. Shaked, P. M. Keene, J. C. Rodriguez, F. F. Owen, R. L. Hitterman, J. D. Jorgensen, *Crystal Structures of the High-T_C Superconducting Copper-Oxides*, Elsevier Science B.V., Amsterdam, **1994**.
[99] R. A. M. Ram, P. Ganguly, C. N. R. Rao, *J. Solid State Chem.* **1987**, *70*, 82.
[100] J. B. MacChesney, J. F. Potter, R. C. Sherwood, *J. Appl. Phys.* **1969**, *40*, 1243.
[101] Y. Moritomo, A. Asamitsu, H. Kuwahara, Y. Tokura, *Nature* **1996**, *380*, 141.
[102] R. Mahesh, R. Mahendiran, A. K. Raychaudhuri, C. N. R. Rao, *J. Solid State Chem.* **1996**, *122*, 448.
[103] R. Seshadri, C. Martin, M. Hervieu, B. Raveau, C. N. R. Rao, *Chem. Mater.* **1997**, *9*, 270.
[104] P. D. Battle, S. J. Blundell, M. A. Green, W. Hayes, H. Honold, A. K. Klehe, N. S. Laskey, J. E. Millburn, L. Murphy, M. J. Rosseinsky, N. A. Samarin, J. Singleton, N. E. Sluchanko, S. P. Sullivan, J. F. Vente, *J. Phys. Condens. Matter* **1996**, *8*, L427.
[105] P. D. Battle, M. A. Green, N. S. Laskey, J. E. Millburn, L. Murphy, M. J. Rosseinsky, S. P. Sullivan, J. F. Vente, *Chem. Mater.* **1997**, *9*, 552.
[106] P. Laffez, G. V. Tendeloo, R. Seshadri, M. Hervieu, C. Martin, A. Maignan, B. Raveau, *J. Appl. Phys.* **1996**, *80*, 5850.
[107] R. Seshadri, C. Martin, A. Maignan, M. Hervieu, B. Raveau, C. N. R. Rao, *J. Mater. Chem.* **1996**, *6*, 1585.
[108] D. N. Argyriou, J. F. Mitchell, J. B. Goodenough, O. Chmaissem, S. Short, J. D. Jorgensen, *Phys. Rev. Lett.* **1997**, *78*, 1568.
[109] J. F. Mitchell, D. N. Argyriou, J. D. Jorgensen, D. G. Hinks, C. D. Potter, S. D. Bader, *Phys. Rev. B* **1997**, *55*, 63.
[110] R. Seshadri, A. Maignan, M. Hervieu, N. Nguyen, B. Raveau, *Solid State Commun.* **1997**, *101*, 453.
[111] R. Seshadri, A. Maignan, C. Martin, F. Letouzé, B. Raveau, *Phys. Rev. B* **1997**, *56*, 5504.
[112] C. Felser, R. Seshadri, A. Leist, W. Tremel, *J. Mater. Chem.* **1998**, *8*, 787.
[113] N. Mannella, W. L. Yang, X. J. Zhou, H. Zheng, J. F. Mitchell, J. Zaanen, T. P. Devereaux, N. Nagaosa, Z. Hussain, Z.-X. Shen, *Nature* **2005**, *438*, 474.
[114] D. J. Singh, *Phys. Rev. B* **1997**, *55*, 313.
[115] D. J. Singh, W. E. Pickett, *Physica C* **1992**, *203*, 193.
[116] Z. Zeng, M. Greenblatt, J. E. Sunstrom, M. Croft, *J. Solid State Chem.* **1999**, *147*, 185.
[117] T. Hagino, Y. Seki, N. Wada, S. Tsuji, T. Shirane, K.-i. Kumagai, S. Nagata, *Phys. Rev. B* **1995**, *51*, 12673.

[118] V. Tsurkan, M. Mucksch, V. Fritsch, J. Hemberger, M. Klemm, S. Klimm, S. Korner, H.-A. Krug von Nidda, D. Samusi, E.-W. Scheidt, A. Loidl, S. Horn, R. Tidecks, *Phys. Rev. B* **2003**, *68*, 134434.
[119] K. Ahn, C. Felser, R. Seshadri, R. K. Kremer, A. Simon, *J. Alloys Compd.* **2000**, *303–304*, 252.
[120] I. Eremin, P. Thalmeier, P. Fulde, R. K. Kremer, K. Ahn, A. Simon, *Phys. Rev. B* **2001**, *64*, 064425.
[121] T. Maitra, A. Taraphder, A. N. Yaresko, P. Fulde, *Eur. Phys. J. B* **2006**, *49*, 433.
[122] M. Ryazanov, A. Simon, R. K. Kremer, H. Mattausch, *Phys. Rev. B* **2005**, *72*, 092408.
[123] F. Holtzberg, S. von Molnar, J. M. D. Coey, *Handb. Semicond.* **1980**, *3*, 815.
[124] P. Wachter, *Crit. Rev. Solid State Sci.* **1972**, *3*, 189.
[125] L. Esaki, P. J. Stiles, S. von Molnar, *Phys. Rev. Lett.* **1967**, *19*, 852.
[126] Y. Shapira, S. Foner, T. B. Reed, *Phys. Rev. B* **1973**, *8*, 2299.
[127] J. Lettieri, V. Vaithyanathan, S. K. Eah, J. Stephens, V. Sih, D. D. Awschalom, J. Levy, D. G. Schlom, *Appl. Phys. Lett.* **2003**, *83*, 975.
[128] H. Ott, S. J. Heise, R. Sutarto, Z. Hu, C. F. Chang, H. H. Hsieh, H.-J. Lin, C. T. Chen, L. H. Tjeng, *Phys. Rev. B* **2006**, *73*, 094407.
[129] C. Felser, *J. Alloys Compd.* **1997**, *262–263*, 87.
[130] K. Westerholt, H. Bach, R. Wendemuth, S. Methfessel, *Solid State Commun.* **1979**, *31*, 961.
[131] H. Oharaa, S. Sasaki, Y. Konoikea, T. Toyodaa, K. Yamawakia, M. Tanakab, *Phys. B* **2004**, *350*, 353.
[132] J. Kauzlarich, J. Olmstead, M. M. Kauzlarich, S. M. Lee, P. Klavins, Z. Fisk, *Inorg. Chem.* **2005**, *44*, 5322.
[133] I. Tsubokawa, *J. Phys. Soc. Jpn.* **1960**, *15*, 1664.
[134] H. Chiba, T. Atou, Y. Syono, *J. Solid State Chem.* **1997**, *132*, 139.
[135] K. Kohn, K. Inoue, O. Horie, S. Akimoto, *J. Solid State Chem.* **1976**, *18*, 27.
[136] J. D. Garrett, J. E. Greedan, D. A. MacLean, *Mater. Res. Bull.* **1981**, *16*, 145.
[137] C. M. Fang, G. A. de Wijs, R. A. de Groot, *J. Appl. Phys.* **2002**, *91*, 8340.
[138] T. Dietl, H. Ohno, F. Matsukura, J. Cibert, D. Ferrand, *Science* **2000**, *287*, 1019.
[139] S. A. Chambers, R. F. C. Farrow, *MRS Bull.* **2003**, 729.
[140] Y. Matsumoto, M. Murakami, T. Shono, T. Hasegawa, T. Fukumura, M. Kawasaki, P. Ahmet, T. Chikyow, S.-y. Koshihara, H. Koinuma, *Science* **2001**, *291*, 854.
[141] S. A. Chambers, T. Droubay, C. M. Wang, A. S. Lea, R. F. C. Farrow, L. Folks, V. Deline, S. Anders, *Appl. Phys. Lett.* **2003**, *82*, 1257.
[142] K. Sato, H. Katayama-Yoshida, *Jpn. J. Appl. Phys. Part 2* **2000**, *39*, L555.
[143] N. A. Spaldin, *Phys. Rev. B* **2004**, *69*, 125201.
[144] T. Fukumura, Z. Jin, M. Kawasaki, T. Shono, T. Hasegawa, S. Koshihara, H. Koinuma, *Appl. Phys. Lett.* **2001**, *78*, 958.
[145] S. Kolesnik, B. Dabrowski, J. Mais, *J. Supercond.* **2002**, *15*, 251.
[146] S. W. Yoon, S.-B. Cho, S. C. We, S. Yoon, B. J. Suh, H. K. Song, Y. J. Shin, *J. Appl. Phys.* **2002**, *93*, 7879.
[147] W. H. Brumage, C. F. Dorman, C. R. Quade, *Phys. Rev. B* **2001**, *63*, 104411.
[148] S. Kolesnik, B. Dabrowksi, J. Mais, *J. Appl. Phys.* **2003**, *95*, 2582.
[149] A. S. Risbud, N. A. Spaldin, Z. Q. Chen, S. Stemmer, R. Seshadri, *Phys. Rev. B* **2003**, *68*, 205202.
[150] J. H. Kim, H. Kim, D. Kim, Y. E. Ihm, W. K. Choo, *J. Appl. Phys.* **2002**, *92*, 6066.
[151] P. Sharma, A. Gupta, F. J. Owens, K. V. Rao, R. Sharma, R. Ahuja, J. M. O. Guillen, B. Johannson, G. A. Gehring, *Nat. Mater.* **2003**, *2*, 673.
[152] D. A. Schwartz, N. S. Norberg, Q. P. Nguyen, J. M. Parker, D. R. Gamelin, *J. Am. Chem. Soc.* **2003**, *125*, 13205.
[153] G. H. Lee, S. H. Huh, J. W. Jeong, B. J. Choi, S. H. Kim, H.-C. Ri, *J. Am. Chem. Soc.* **2002**, *124*, 12094.
[154] G. Lawes, A. S. Risbud, A. P. Ramirez, R. Seshadri, *Phys. Rev. B* **2005**, *71*, 045201.
[155] C. N. R. Rao, F. L. Deepak, *J. Mater. Chem.* **2005**, *15*, 573.
[156] S. Deka, R. Pacricha, P. A. Joy, *Phys. Rev. B* **2006**, *74*, 033201.
[157] S. G. Yang, T. Li, B. X. Gu, Y. W. Du, H. Y. Sung, S. T. Hung, C. Y. Wong, A. B. Pakhomov, *Appl. Phys. Lett.* **2003**, *83*, 3746.
[158] H. Akinaga, M. Mizuguchi, K. Ono, M. Oshima, *J. Magn. Soc. Jpn.* **2000**, *22*, 451.
[159] H. Akinaga, T. Manago, M. Shirai, *Jpn. J. Appl. Phys. Part 2* **2000**, *39*, L1118.
[160] I. Galanakis, P. Mavropoulos, *Phys. Rev. B* **2003**, *67*, 104417.
[161] M. Penicaud, B. Silberchiot, C. B. Sommers, J. Kubler, *J. Magn. Magn. Mater.* **1992**, *103*, 212.
[162] C. Ritter, M. R. Ibarra, L. Morellon, J. Blasco, J. Garcia, J. M. D. Teresa, *J. Phys. Condens. Matter* **2000**, *12*, 8295.
[163] H. Asano, N. Kozuka, A. Tsuzuki, M. Matsui, *Appl. Phys. Lett.* **2004**, *85*, 263.
[164] M. Retuerto, J. A. Alonso, M. J. Martínez-Lope, J. L. Martínez, M. García-Hernández, *Appl. Phys. Lett.* **2004**, *85*, 266.
[165] Y. Sui, X. J. Wang, Z. N. Qian, J. G. Cheng, Z. G. Liu, J. P. Miao, Y. Li, W. H. Su, C. K. Ong, *Appl. Phys. Lett.* **2004**, *85*, 269.
[166] A. Jung, I. Bonn, V. Ksenofontov, G. Melnyk, J. Ensling, C. Felser, W. Tremel, *J. Mater. Chem.* **2005**, *15*, 1760.
[167] A. Jung, V. Ksenovontov, S. Reiman, C. Felser, W. Tremel, *Phys. Rev. B* **2006**, *73*, 144414.
[168] Y. Krockenberg, K. Mogare, M. Reehuis, M. Tovar, M. Jansen, G. Vaitheeswaran, V. Kanchana, F. Bultmark, A. Delin, F. Wilhelm, A. Rogalev, A. Winkler, L. Alff, *Phys. Rev. B* **2006**, submitted.
[169] K. Schwarz, *J. Phys.* **1986**, *16*, 211.
[170] B. L. Chamberland, *CRC Crit. Rev. Solid State Sci.* **1977**, *7*, 1.
[171] M. S. Laad, L. Craco, E. Müller-Hartmann, *Phys. Rev. B* **2001**, *64*, 214421.
[172] S. M. Watts, S. Wirth, S. von Molnar, A. Barry, J. M. D. Coey, *Phys. Rev. B* **2000**, *61*, 9621.
[173] Y. Ji, G. J. Strijkers, F. Y. Yang, C. L. Chien, J. M. Byers, A. Anguelouch, G. Xiao, A. Gupta, *Phys. Rev. Lett.* **2001**, *86*, 5585.
[174] J. S. Parker, S. M. Watts, P. G. Ivanov, P. Xiong, *Phys. Rev. Lett.* **2002**, *88*, 196601.
[175] R. S. Keizer, S. T. Goennenwein, T. M. Klapwijk, G. Miao, G. Xiao, A. Gupta, *Nature* **2006**, *439*, 825.
[176] F. S. Bergeret, A. F. Volkov, K. B. Efetov, *Phys. Rev. Lett.* **2001**, *86*, 4096.
[177] D. C. Johnston, H. Prakash, W. H. Zachariasen, R. Viswanathan, *Mater. Res. Bull.* **1973**, *8*, 777.
[178] S. Kondo, D. C. Johnston, C. A. Swenson, F. Borsa, A. V. Mahajan, L. L. Miller, T. Gu, A. I. Goldman, M. B. Maple, D. A. Gajewski, E. J. Freeman, N. R. Dilley, R. P. Dickey, J. Merrin, K. Kijima, G. M. Luke, Y. J. Uemura, O. Chmaissem, J. D. Jorgensen, *Phys. Rev. Lett.* **1997**, *78*, 3729.
[179] P. G. Bruce, *Philos. Trans. R. Soc. London Ser. A* **1996**, 354, 1577.
[180] J. B. Goodenough, *Solid State Ionics* **1994**, *69*, 184.
[181] D. Guyomard, J.-M. Tarascon, *Solid State Ionics* **1994**, *69*, 222.
[182] M. M. Thackeray, *J. Electrochem. Soc.* **1995**, *142*, 2558.
[183] J. Rodríguez-Carvajal, G. Rousse, C. Masquelier, M. Hervieu, *Phys. Rev. Lett.* **1998**, *81*, 4660.
[184] E. J. W. Verweij, P. W. Haaymann, *Physica* **1941**, *8*, 979.
[185] Y. Dedkov, U. Rüdiger, G. Güntherodt, *Phys. Rev. B* **2002**, *65*, 064417.
[186] R. Basu, C. Felser, A. Maignanc, R. Seshadri, *J. Mater. Chem.* **2000**, *10*, 1921.

[187] M. Lauer, R. Valenti, H. C. Kandpal, R. Seshadri, *Phys. Rev. B* **2004**, *69*, 075117.
[188] J. I. Horikawa, T. Hamajima, F. Ogata, T. Kambara, K. I. Gondaira, *J. Phys. C* **1982**, *15*, 2613.
[189] K. E. M. Hanssen, P. E. Mijnarends, *Phys. Rev. B* **1986**, *34*, 5009.
[190] K. E. M. Hanssen, P. E. Mijnarends, L. P. L. M. Rabou, K. H. J. Buschow, *Phys. Rev. B* **1990**, *42*, 1533.
[191] J. S. Correa, C. Eibl, G. Rangelov, J. Braun, M. Donath, *Phys. Rev. B* **2006**, *73*, 125316.
[192] W. Zhu, B. Sinkovic, E. Vescovo, C. Tanaka, J. S. Moodera, *Phys. Rev. B* **2001**, *64*, R060403.
[193] R. Meservey, P. M. Tedrow, *Phys. Rep.* **1994**, *238*, 173.
[194] S. Suga, S. Imada, *J. Electron Spectrosc. Relat. Phenom.* **1998**, 92, 1.
[195] K. H. J. Buschow, P. G. van Engen, *J. Magn. Magn. Mater.* **1981**, *25*, 90.
[196] R. Weht, W. E. Pickett, *Phys. Rev. B* **1999**, *60*, 13006.
[197] M. D. Bojin, R. Hoffmann, *Helv. Chim. Acta* **2003**, *86*, 1653.
[198] S. Baran, J. Leciejewicz, N. Stüsser, A. Szytua, A. Zygmunt, V. Ivanov, *J. Phys. Condens. Matter* **1996**, *8*, 8397.
[199] S. Baran, J. Leciejewicz, N. Stüsser, A. Szytua, Z. Tomkowicz, *Solid State Commun.* **1997**, *101*, 631.
[200] S. Baran, J. Leciejewicz, M. Slaski, P. Hofmann, A. Szytula, *J. Alloys Compd.* **1998**, *275–277*, 541.
[201] S. Baran, M. Hofmann, J. Leciejewicz, M. Slaski, A. Szytula, A. Zygmunt, *J. Phys. Condens. Matter* **1997**, *9*, 9053.
[202] D. Bialic, R. Kruk, R. Kmieć, K. Tomala, *J. Alloys Compd* **1997**, *257*, 49.
[203] I. Galanakis, P. H. Dederichs, N. Papanikolaou, *Phys. Rev. B* **2002**, *66*, 174429.
[204] S. Picozzi, A. Continenza, A. J. Freeman, *Phys. Rev. B* **2002**, *66*, 094421.
[205] I. Galanakis, P. H. Dederichs, N. Papanikolaou, *Phys. Rev. B* **2002**, *66*, 134428.
[206] Y. Miura, K. Nagao, M. Shirai, *Phys. Rev. B* **2004**, *69*, 144413.
[207] S. Wurmehl, G. H. Fecher, K. Kroth, F. Kronast, H. A. Dürr, Y. Takeda, Y. Saitoh, K. Kobayashi, H.-J. Lin, G. Schönhense, C. Felser, *J. Phys. D* **2006**, *39*, 803.
[208] M. Zhang, Z. Liu, H. Hu, G. Liu, Y. Cui, J. Chen, G. Wu, X. Zhang, G. Xiao, *J. Magn. Magn. Mater.* **2004**, *277*, 30.
[209] K. Kobayashi, R. Y. Umetsu, R. Kainuma, K. Ishida, T. Oyamada, A. Fujita, K. Fukamichi, *Appl. Phys. Lett.* **2004**, *85*, 4684.
[210] E. Clifford, M. Venkatesan, R. Gunning, J. M. D. Coey, *Solid State Commun.* **2004**, *131*, 61.
[211] I. Galanakis, *J. Phys. Condens. Matter* **2004**, *16*, 8007.
[212] H.-J. Elmers, G. H. Fecher, D. Valdaitsev, S. A. Nepijko, A. Gloskovskii, G. Jakob, G. Schönhense, S. Wurmehl, T. Block, C. Felser, P.-C. Hsu, W.-L. Tsai, S. Cramm, *Phys. Rev. B* **2003**, *67*, 104412.
[213] C. Felser, H.-J. Elmers, G. H. Fecher, *Lecture Notes in Physics*, *Vol. 667*, Springer, Berlin, **2005**.
[214] P. J. Webster, *J. Phys. Chem. Solids* **1971**, *32*, 1221.
[215] P. J. Webster, K. R. A. Ziebeck, *J. Phys. Chem. Solids* **1973**, *34*, 1647.
[216] V. Niculescu, J. I. Budnick, W. A. Hines, K. Rajt, S. Pickart, S. Skalski, *Phys. Rev. B* **1979**, *19*, 452.
[217] V. Niculescu, T. J. Burch, K. Raj, J. I. Budnick, *J. Magn. Magn. Mater.* **1977**, *5*, 60.
[218] S. Wurmehl, G. H. Fecher, H. C. Kandpal, V. Ksenofontov, C. Felser, H.-J. Lin, *Appl. Phys. Lett.* **2006**, *88*, 032503.
[219] S. Ishida, S. Akazawa, Y. Kubo, J. Ishida, *J. Phys. F* **1982**, *12*, 1111.
[220] L. Hedin, B. I. Lundqvist, *J. Phys. C* **1971**, *4*, 2064.
[221] W. Kohn, L. J. Sham, *Phys. Rev.* **1965**, *140*, 1133.
[222] U. von Barth, L. Hedin, *J. Phys. C* **1972**, *5*, 1629.
[223] S. H. Vosko, L. Wilk, M. Nusair, *Can. J. Phys.* **1980**, *58*, 1200.
[224] S. Ishida, S. Fujii, S. Kashiwagi, S. Asano, *J. Phys. Soc. Jpn.* **1995**, *64*, 2152.
[225] S. Ishida, S. Kashiwagi, S. Fujii, S. Asano, *Physica B* **1995**, *210*, 140.
[226] P. Mohn, P. Blaha, K. Schwarz, *J. Magn. Magn. Mater.* **1995**, *140–144*, 183.
[227] J. P. Perdew, K. Burke, M. Ernzerhof, *Phys. Rev. Lett.* **1996**, *77*, 3865.
[228] J. P. Perdew, K. Burke, M. Ernzerhof, *Phys. Rev. Lett.* **1997**, *78*, 1396.
[229] J. P. Perdew, J. A. Chevary, S. H. Vosko, K. A. Jackson, M. R. Pederson, D. J. Singh, C. Fiolhais, *Phys. Rev. B* **1992**, *46*, 6671.
[230] J. P. Perdew, W. Yue, *Phys. Rev. B* **1986**, *33*, 8800.
[231] V. N. Antonov, H. A. Dürr, Y. Kucherenko, L. V. Bekenov, A. N. Yaresko, *Phys. Rev. B* **2005**, *72*, 054441.
[232] J. C. Slater, *Phys. Rev.* **1936**, *49*, 931.
[233] J. H. van Vleck, *Rev. Mod. Phys.* **1945**, *17*, 27.
[234] J. H. van Vleck, *Rev. Mod. Phys.* **1953**, *25*, 220.
[235] J. E. Goldman, *Rev. Mod. Phys.* **1953**, *25*, 108.
[236] P. Fulde, *Electron Correlations in Molecules and Solids*, 3rd ed., Springer, Heidelberg, **1995**.
[237] V. I. Anisimov, F. Aryasetiawan, A. I. Lichtenstein, *J. Phys. Condens. Matter* **1997**, *9*, 767.
[238] H. C. Kandpal, G. H. Fecher, C. Felser, G. Schönhense, *Phys. Rev. B* **2006**, *73*, 094422.
[239] T. Bandyopadhyay, D. D. Sarma, *Phys. Rev. B* **1989**, *39*, 3517.
[240] B. Balke, G. H. Fecher, H. C. Kandpal, C. Felser, *Phys. Rev. B* **2006**, *74*, 104405.
[241] G. H. Fecher, A. Gloskowskii, K. Kroth, J. Barth, B. Balke, C. Felser, F. Schaefers, M. Mertin, W. Eberhardt, S. Maehl, O. Schaff, *J. Electron Spectrosc. Relat. Phenom.* **2006**, in press; G. H. Fecher, B. Balke, S. Ouardi, C. Felser, *J. Phys. D: Appl. Phys.* **2006**, in press.
[242] J. Schmalhorst, S. Kämmerer, G. Reiss, A. Hütten, *Appl. Phys. Lett.* **2005**, *86*, 052501.
[243] J. Schmalhorst, S. Kämmerer, M. Sacher, G. Reiss, A. Hütten, A. Scholl, *Phys. Rev. B* **2004**, *70*, 024426.
[244] P. LeClair, H. J. M. Swagten, J. T. Kohlhepp, W. J. M. de Jonge, *Appl. Phys. Lett.* **2000**, *76*, 3783.
[245] K. Inomata, S. Okamura, R. Goto, N. Yezuka, *Jpn. J. Appl. Phys.* **2003**, *42*, L419.
[246] K. Inomata, S. Okamura, N. Tezuka, *J. Magn. Magn. Mater.* **2004**, *282*, 269.
[247] G. Jakob, F. Casper, V. Beaumont, S. Falk, N. Auth, H.-J. Elmers, C. Felser, H. Adrian, *J. Magn. Magn. Mater.* **2005**, *290–291*, 1104.
[248] A. Conca, S. Falk, G. Jakob, M. Jourdan, H. Adrian, *J. Magn. Magn. Mater.* **2005**, *290–291*, 1127.
[249] T. Marukame, T. Ishikawa, K. Matsuda, T. Uemura, M. Yamamoto, *Appl. Phys. Lett.* **2006**, *88*, 262503
[250] N. Ikeda, N. Tezuka, S. Sugimoto, K. Inomata, presented at the 30th Annual Conference on Magnetics in Japan, **2006**.
[251] Y. Sakuraba, M. Hattori, M. Oogane, Y. Ando, H. Kato, A. Sakuma, T. Miyazaki, H. Kubota, *Appl. Phys. Lett.* **2006**, *88*, 192508.
[252] Y. Sakuraba, T. Miyakoshi, M. Oogane, Y. Ando, A. Sakuma, T. Miyazaki, H. Kubota, *Appl. Phys. Lett.* **2006**, *89*, 052508.
[253] K. Endo, M. Tokiyama, H. Matsuda, K. Ooiwa, T. Goto, J. Arai, *J. Phys. Soc. Jpn.* **2004**, *73*, 1944.
[254] J. Tobola, S. Kaprzyk, P. Pecheur, *Phys. Status Solidi B* **2003**, *236*, 531.
[255] K. Endo, H. Matsuda, K. Ooiwa, M. Iijima, T. Goto, K. Sato, I. Umehara, *J. Magn. Magn. Mater.* **1998**, *177–181*, 1437.
[256] Y. Nishino, S.-y. Inoue, S. Asano, N. Kawamiya, *Phys. Rev. B* **1993**, *48*, 13607.
[257] S. Majumdar, M. K. Chattopadhyay, V. K. Sharma, K. J. S. Sokhey, S. B. Roy, P. Chaddah, *Phys. Rev. B* **2005**, *72*, 012417.

[258] J. Pierre, I. Karla, K. Kaczmarska, *Physica B* **1999**, *259–261*, 845.
[259] J. Tobola, L. Jodin, P. Pecheur, H. Scherrer, G. Venturini, B. Malaman, S. Kaprzyk, *Phys. Rev. B* **2001**, *64*, 155103.
[260] J. Pierre, K. Kaczmarska, J. Tobola, R. V. Skolozdra, G. A. Melnyk, *Physica B* **1999**, *259–261*, 841.
[261] A. Simon, *J. Supercond.* **2000**, *13*, 691.
[262] P. Blaha, K. Schwarz, G. K. H. Madsen, D. Kvasnicka, J. Luitz, *Wien2k*, *An Augmented Plane Wave + Local Orbitals Program for Calculating Crystal Properties*, Karlheinz Schwarz, Technische Universität Wien, **2001**.
[263] See reference [249].
[264] S. Kämmerer, A. Thomas, A. Hütten, G. Reiss, *Appl. Phys. Lett.* **2004**, *85*, 79.
[265] Y. Sakuraba, J. Nakata, M. Oogane, H. Kubota, Y. Ando, A. Sakuma, T. Miyazaki, *Jpn. J. Appl. Phys.* **2005**, *44*, L1100.
[266] H. Kubota, J. Nakata, M. Oogane, Y. Ando, A. Sakuma, T. Miyazaki, *Jpn. J. Appl. Phys.* **2004**, *43*, L984.
[267] S. Okamura, A. Miyazaki, S. Sugimoto, N. Tezuka, K. Inomata, *Appl. Phys. Lett.* **2005**, *86*, 232503.
[268] K. Inomata, S. Okamura, A. Miyazaki, M. Kikuchi, N. Tezuka, M. Wojcik, E. Jedryka, *J. Phys. D* **2006**, *39*, 816.
[269] N. Tezuka, N. Ikeda, A. Miyazaki, S. Sugimoto, M. Kikuchi, K. Inomata, *Appl. Phys. Lett.* **2006**, *89*, 112514.
[270] I. Karla, J. Pierre, R. V. Skolozdra, *J. Alloys Compd.* **1998**, *265*, 42.
[271] K. Shimizu, T. Kimura, S. Furomoto, K. Takeda, K. Kontani, Y. Onuki, K. Amaya, *Nature* **2001**, *412*, 316.